



Anoxic atmospheres on Mars driven by volcanism: Implications for past environments and life



Steven F. Sholes^{a,*}, Megan L. Smith^a, Mark W. Claire^b, Kevin J. Zahnle^c, David C. Catling^a

^a Department of Earth and Space Sciences and Astrobiology Program, University of Washington, Johnson Hall 070, Box 351310, 4000 15th Avenue NE, Seattle, WA 98195, USA

^b Department of Earth and Environmental Sciences, University of St. Andrews, Irvine Building, St. Andrews, Fife KY16 9AL, UK

^c Space Sciences Division, MS 245-3, NASA Ames Research Center, Moffett Field, CA 94035, USA

ARTICLE INFO

Article history:

Received 18 April 2016

Revised 13 February 2017

Accepted 23 February 2017

Available online 1 March 2017

Keywords:

Mars atmosphere

Volcanism

Photochemistry

Sulfur

Atmosphere chemistry

ABSTRACT

Mars today has no active volcanism and its atmosphere is oxidizing, dominated by the photochemistry of CO₂ and H₂O. Mars experienced widespread volcanism in the past and volcanic emissions should have included reducing gases, such as H₂ and CO, as well as sulfur-bearing gases. Using a one-dimensional photochemical model, we consider whether plausible volcanic gas fluxes could have switched the redox-state of the past martian atmosphere to reducing conditions. In our model, the total quantity and proportions of volcanic gases depend on the water content, outgassing pressure, and oxygen fugacity of the source melt. We find that, with reasonable melt parameters, the past martian atmosphere (~3.5 Gyr to present) could have easily reached reducing and anoxic conditions with modest levels of volcanism, >0.14 km³ yr⁻¹, which are well within the range of estimates from thermal evolution models or photogeological studies. Counter-intuitively we also find that more reducing melts with lower oxygen fugacity require greater amounts of volcanism to switch a paleo-atmosphere from oxidizing to reducing. The reason is that sulfur is more stable in such melts and lower absolute fluxes of sulfur-bearing gases more than compensate for increases in the proportions of H₂ and CO. These results imply that ancient Mars should have experienced periods with anoxic and reducing atmospheres even through the mid-Amazonian whenever volcanic outgassing was sustained at sufficient levels. Reducing anoxic conditions are potentially conducive to the synthesis of prebiotic organic compounds, such as amino acids, and are therefore relevant to the possibility of life on Mars. Also, anoxic reducing conditions should have influenced the type of minerals that were formed on the surface or deposited from the atmosphere. We suggest looking for elemental polysulfur (S₈) as a signature of past reducing atmospheres. Finally, our models allow us to estimate the amount of volcanically sourced atmospheric sulfate deposited over Mars' history, approximately ~10⁶–10⁹ Tmol, with a spread depending on assumed outgassing rate history and magmatic source conditions.

© 2017 Elsevier Inc. All rights reserved.

1. Introduction

The modern martian atmosphere is oxidizing but the atmosphere on past Mars could have had significantly different chemistry and may have even been anoxic when there was a large input of volcanic gases (Catling and Moore, 2003; Zahnle et al., 2008). Today, there is no detectable volcanic input (Krasnopolsky, 2005) and the photochemistry of the atmosphere is dominated by CO₂, H₂O, and their photochemical byproducts (Krasnopolsky and Lefevre, 2013; Mahaffy et al., 2013; Zahnle et al., 2008). However, extinct volcanoes and volcanic terrains indicate that

Mars experienced widespread volcanism in the past (Carr and Head, 2010; Greeley and Spudis, 1981) which would have injected reducing gases into the atmosphere, in addition to CO₂ and H₂O. The reducing volcanic gases, such as CO and H₂, would have reacted with oxidants and may have switched the redox chemistry of the atmosphere from oxidizing to reducing, depending on their proportions relative to CO₂ and H₂O in outgassing.

Planetary atmospheres can be categorized into two meaningful chemical endmembers: reducing and oxidizing. Reducing atmospheres are those in which oxidation is limited or prohibited and therefore elements like carbon and sulfur are more likely to be found in their hydrogenated reduced forms (e.g. CH₄, H₂S) than their oxidized forms (e.g. CO₂, SO₂). Oxidizing atmospheres are the reverse. Highly reducing atmospheres can become anoxic with non-zero but negligible oxygen levels.

* Corresponding author.

E-mail address: sfsholes@uw.edu (S.F. Sholes).

The possibility that Mars had anoxic and reducing conditions is of considerable interest, not only for understanding the evolution of planetary atmospheres, but also in the creation of habitable environments. Reducing and anoxic atmospheres are much more favorable to prebiotic chemistry than oxidizing ones (e.g. Urey, 1952). These conditions enable photochemistry to create prebiotic organics (e.g. amino acids), which have been discussed in the context of the origin of life on Earth (e.g. Kasting, 1993). Very hydrogen-rich atmospheres can also provide greenhouse warming on early Mars through collision-induced absorption (Batalha et al., 2015; Ramirez et al., 2014; Sagan, 1977).

Terrestrial volcanic gases are weakly reducing, composed dominantly of oxidized gases (CO_2 , H_2O , and SO_2), minor amounts of reducing gases (H_2 , H_2S , and CO), and traces of other gases (S_2 , HCl , HF , OCS , and SO) (Symonds et al., 1994), whereas volcanic gases on ancient Mars are of uncertain redox state but were almost certainly more sulfur-rich (Wänke and Dreibus, 1994). The magnitude and proportions of volcanic gases on Mars would have depended on the chemical state of martian magmas: the redox state, water content, and abundance of other species such as sulfur and carbon (Gaillard et al., 2013; Gaillard and Scaillet, 2009).

Mars is sulfur rich compared to Earth, with upwards of 3–4 times as much sulfur in Mars' mantle than in Earth's (Gaillard and Scaillet, 2009; Gendrin et al., 2005; McSween, 1994; Yen et al., 2005). This has led to Mars having an active sulfur cycle that would have affected the surface environment (King and McLennan, 2010). Sulfate deposits are abundant on Mars, and sulfate in soils or rocks has been found at the sites of the Viking landers (Toulmin et al., 1977), Mars Exploration Rovers (Squyres et al., 2004), Phoenix (Kounaves et al., 2010), and Mars Science Laboratory (Mahaffy et al., 2013). These sulfur deposits could originate from the weathering of sulfides in surficial basalts (Burns and Fisher, 1993; King and McSween, 2005) or from volcanic gases (Settle, 1979; Smith et al., 2014). Sulfate in some martian meteorites shows mass independent isotope fractionations of sulfur which, although modest in magnitude compared to what is seen from the Archean Earth, suggest cycling of sulfur gases through the atmosphere (Farquhar et al., 2007). It is likely that a considerable amount of sulfur on the surface of Mars originated in volcanic outgassing (primarily in the form of SO_2), which was then oxidized and hydrated in the atmosphere to form sulfate aerosols (H_2SO_4) (McGouldrick et al., 2011; Settle, 1979).

The role sulfur plays in the atmospheric chemistry of Mars has been studied mainly for how it might have affected the climate. Some past work suggested that sulfur in the form of SO_2 could have acted as a prominent greenhouse gas in the past (Halevy et al., 2007; Johnson et al., 2008b; Johnson et al., 2009; Postawko and Kuhn, 1986). However, such studies neglected the effect of sulfate aerosols. Models that include sulfate aerosols find that the increased planetary albedo more than offsets the increased greenhouse effect, so that the net effect of adding SO_2 is to cool Mars' surface (Tian et al., 2010). This latter result is consistent with expectations based on what we know of Earth and Venus: volcanic sulfur aerosols cool the Earth (Robock, 2000) and contribute to the very large albedo of Venus (Toon et al., 1982). Others have found that it is possible to construct sulfate aerosols of dust coated with sulfate that can warm Mars (Halevy and Head, 2014), but whether such particles existed is unknown. Additionally, this study did not account for horizontal heat transport (Wordsworth et al., 2015) or elemental sulfur aerosols which would also contribute to cooling (Tian et al., 2010).

Volcanic S-containing gases have a reducing effect when injected into an oxidizing atmosphere because sulfur is removed from the atmosphere in its most oxidized form as sulfate. These sulfur-bearing gas species provide a source material for the sulfate deposits on the surface and also a sink for oxidizing species in the

atmosphere when sulfate aerosols form. In reducing atmospheres sulfur can also be removed as elemental sulfur (S_8), or as a sulfide, both of which are more reduced than SO_2 (Pavlov and Kasting, 2002; Zahnle et al., 2006). Combined with other reducing gases from volcanic input (e.g. H_2 or CO), large amounts of sulfur gases on ancient Mars may have created anoxic conditions in the atmosphere.

In this paper, we model the martian atmosphere using an updated one-dimensional photochemical code (Catling et al., 2010; Smith et al., 2014; Zahnle et al., 2008) to determine whether past martian atmospheres could have been anoxic given plausible mantle buffers and outgassing rates. We simulate increasing extrusive volcanic activity to determine where the model reaches the tipping point from an oxidizing atmosphere (where the redox state is governed by H-escape) to a neutral or reduced atmosphere (where the redox state is governed by volcanoes). We then discuss the implications of the modeled environments in the context of possible future observables. Finally, we describe the implications for habitability of Mars.

2. Methods

To investigate the effects of volcanic gases on atmospheric chemistry, we use a one-dimensional photochemical model originally developed by Kasting (1979) for the early Earth. The code has since been modified and validated with the known bulk composition of the modern martian atmosphere (see Franz et al., 2015 for modern bulk composition). It has been applied to past martian atmospheres with oxygen, carbon, and hydrogen (O–C–H) chemistry (Zahnle et al., 2008). Sulfur, chlorine, and nitrogen chemistry were applied and validated against observations in a version of the code used for the modern Earth (Catling et al., 2010). Here we use a combined version that contains carbon, hydrogen, oxygen, nitrogen, and sulfur (C–H–O–N–S) chemistry developed for Mars, following Smith et al. (2014). We present a table of S reactions, which were omitted from the aforementioned studies, in Appendix A. This list has been updated to include 25 reactions to be consistent with other photochemical models (Domagal-Goldman et al., 2011; Zahnle et al., 2016). While chlorine is an important minor volcanic gas, and is outgassed in small amounts primarily as HCl on Earth, we chose to use a version of the model without chlorine species primarily because of their very minor role in overall atmospheric redox for modern Mars (Smith et al., 2014).

In our model, volcanic gases are assumed to flux into background atmospheric conditions similar to modern Mars so that we could assess the shift from a modern atmosphere to ancient atmospheres that may have occurred since the early Amazonian/late Hesperian boundary when Mars was volcanically active but the atmosphere was probably thin (Catling, 2009). Given the uncertainties in the chronostratigraphic epochs, we extend our model only to the past 3.5 Gyr, which is the earliest estimate for the start of the Amazonian (Hartmann, 2005; Werner and Tanaka, 2011).

CO_2 and H_2O vapor, while important volcanic gases on Earth, are held at constant mixing ratios for Mars (H_2O vapor is only held constant in the daytime convective zone). This is done primarily for ease and these gases are assumed to be replenished by and deposited into large surface and subsurface reservoirs. Atmospheric pressure is set to approximately present day levels of 6.5 mbar. The temperature profile follows Zahnle et al. (2008) with surface temperature, T_0 , set to 211 K, which is close to a modern global mean value.

We impose a surface sink on all but the most abundant gas species in the form of a deposition velocity at the lower boundary layer. Unless otherwise stated, we follow Zahnle et al. (2008) and assign all chemically active species a deposition velocity (v_{dep}) of 0.02 cm s^{-1} except for O_2 and H_2 , which are given a $v_{\text{dep}} =$

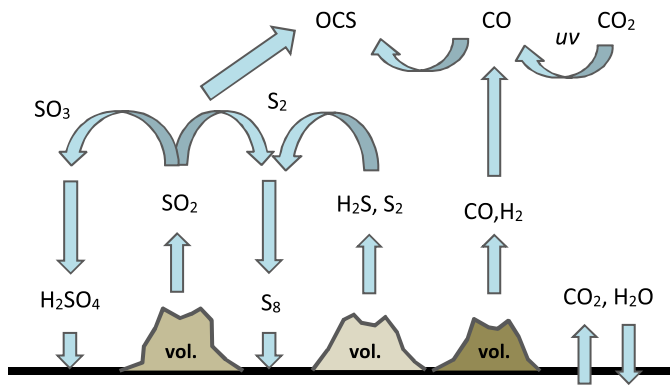


Fig. 1. Schematic diagram showing the dominant sulfur photochemistry and pathways during volcanically-active Mars; ‘vol.’ indicates a volcano. Based on likely magma chemistry (see text) the most important volcanic sulfur gas is generally SO_2 . Atmospheric oxidation reactions turn SO_2 , H_2S , and S_2 into sulfuric acid aerosols, while photochemistry in reducing atmospheres also makes polysulfur aerosols (S_8). Additionally, there is direct deposition of SO_2 to the surface as another sink on S. H_2O and CO_2 concentrations are assumed to be buffered by large subsurface and surface reservoirs. Carbonyl sulfide (OCS) is able to build up through reactions with sulfur-bearing compounds and CO.

0 cm s^{-1} . Unlike previous models, we also assume v_{dep} of OCS is 0 cm s^{-1} (see Appendix B). CO deposition is more complex. There is no known abiotic dry surface sink of CO, therefore $v_{\text{dep,CO}}$ has historically been set to 0 cm s^{-1} . Modeled atmospheres with high-outgassing rates of CO can readily reach instability via the well-known ‘CO-runaway’ effect (e.g. Zahnle et al., 2008), where the atmospheres are unstable against perturbations. A small deposition velocity on CO of $\sim 1 \times 10^{-8} \text{ cm s}^{-1}$ can be assumed if there were large bodies of water on the surface where hydration of dissolved CO forms formate and eventually acetate (Kharecha et al., 2005); and could be as high as $\sim 4 \times 10^{-6} \text{ cm s}^{-1}$ if CO reacts directly with dissolved O_2 (Harman et al., 2015). However, aqueous reactions may only apply during the Noachian-Hesperian when Mars may have experienced long lasting or episodic standing bodies of water, perhaps even as oceans (e.g. Parker et al., 1993). Because we are primarily looking at the Amazonian, we cannot assume large bodies of water. Instead, we consider the fact that the chemistry associated with continual hypervelocity impacts would remove CO.

Impacts have occurred throughout Mars’ history and have affected the atmospheric chemistry. We employ a depositional velocity on CO resulting from the catalytic conversion of CO to methane (CH_4) during hypervelocity impact blasts and one that does not require liquid water at the surface. Kress and McKay (2004) and Sekine et al. (2003) have argued that during large impact blasts from comets and high-iron content meteorites Fischer-Tropsch catalysis reactions provide a sink on atmospheric CO (H_2 can be supplied from dissociated impactor or surficial water/water-ice). From cratering rates, impactor size distributions, and average impact compositions we estimate the average conversion rate of CO to CH_4 , which is a sink on CO that can be expressed as a surface deposition velocity and associated stoichiometric release of CH_4 . Appendix B contains details of our estimations for the deposition velocity of CO and flux of CH_4 . From this, a suitable fixed v_{dep} is of order $10^{-7} \text{ cm s}^{-1}$ for CO, for high-outgassing regimes on Mars.

We implement a corresponding small input flux of CH_4 , of $\sim 1 \times 10^7 \text{ molecules cm}^{-2} \text{ s}^{-1}$, from the Fisher-Tropsch reactions in hypervelocity impacts, which represents a maximum flux under a 1:1 conversion ratio from CO (Appendix B). However, even with this surface flux, $p\text{CH}_4$ is < 3 ppb in all model runs. No volcanic source of methane is imposed, as under the assumed high-temperature volcanic regime CH_4 volcanic fluxes are negligible for all redox states, as is known from measurements from terrestrial volcanoes (Ryan et al., 2006).

The resulting model provides a fit to the modern martian abundances of the important redox-sensitive gases comparable to previous versions. The model is truncated at an altitude of 110 km, with ionospheric chemistry simplified to a downward flux of NO at a rate of $2 \times 10^7 \text{ molecules cm}^{-2} \text{ s}^{-1}$ and an equal flux of CO to preserve redox balance; atomic N also fluxes down at $2 \times 10^6 \text{ molecules cm}^{-2} \text{ s}^{-1}$. We allow hydrogen to escape out through the top of the model at the diffusion-limited rate (Smith et al., 2014; Zahnle et al., 2008).

The model allows for the formation of two sulfur aerosols which are able to precipitate and act as additional sinks on sulfur: elemental polysulfur, S_8 , and sulfate, H_2SO_4 . Fig. 1 is a diagram showing the predominant sulfur photochemistry and pathways. Sulfate aerosols form through the oxidation of the major volcanic gas SO_2 into SO_3 and the subsequent hydration into H_2SO_4 primarily through the following reactions:



In reducing atmospheres, S_8 forms. Sulfur polymerizes into long chains when disulfur (S_2), trisulfur (S_3), and tetrasulfur (S_4) react together, until S_8 is reached. The S_8 allotrope forms a molecular ‘ring’ structure which is conducive to coagulation into aerosol particles. This reaction pathway is unfavorable in oxidizing atmospheres as any S_2 is more readily oxidized into SO and then further oxidized into SO_2 and H_2SO_4 . Additional sources of sulfur for aerosol formation, both S_8 and H_2SO_4 , come from the chemical reaction products involving the oxidation and photolysis of volcanic H_2S and S_2 gases.

Our flux of volcanic gases is scaled according to various estimates of past volcanic outgassing on Mars. Based on photogeologic data, the total magma production for Mars has been estimated as $6.54 \times 10^8 \text{ km}^3$, equivalent to an average of $0.17 \text{ km}^3 \text{ yr}^{-1}$ over the past 3.8 Ga (Greeley and Schneider, 1991). For comparison, the Earth’s magma flux is estimated to be around $26\text{--}34 \text{ km}^3 \text{ yr}^{-1}$ (Greeley and Schneider, 1991). More refined estimates for crustal production rates over time can be inferred using thermal evolution models (e.g. Breuer and Spohn, 2006; Schubert et al., 1992; Xiao et al., 2012) as shown in Fig. 2. The rates range from ~ 0 to $4 \text{ km}^3 \text{ yr}^{-1}$ since the Late Hesperian/Early Amazonian (3.5 Ga). Extrusive volcanic rates modeled by Breuer and Spohn (2006) and Xiao et al. (2012) typically have a peak in the mid-Hesperian to early Amazonian depending on the initial mantle temperature (1800–2000 K), while those modeled by Schubert et al. (1992) show a rapid decline of volcanism with a dependence on a crustal fractionation parameter. The crustal fractionation parameter, χ , used in those calculations is effectively a measure of the efficiency of magma generation in the crust (defined as the ratios of the characteristic mantle convection turnover time and the crustal fractionation time). We test the maximum crustal production rate model of Schubert et al. (1992) ($\chi = 10^{-3}$) to provide an upper limit on their model over the past 3.5 Gyr. Over this time span, their lower rate model is essentially zero which is unlikely given observations. Many of these models show no volcanism in the past 1 Gyr, but volcanism is known to have occurred sporadically within the past 100 Ma on Mars (Werner, 2009). However, these models provide good estimates on average continuous volcanism over time rather than specifically accounting for intermittent periods of volcanism.

The flux of reducing gases depends on the volcanic source region. We cannot in a 1D model simultaneously impose a lower boundary condition that is both a sink (deposition velocity) and a source (a volcanic flux). Thus, as done in previous iterations of

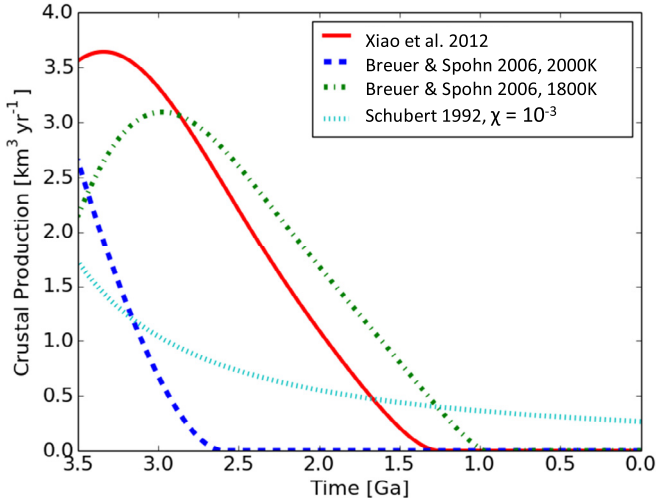


Fig. 2. Estimates of crustal production rates for Mars through time from various authors. Some models suggest that most volcanism should have occurred between the early Noachian and the early Amazonian. In the Breuer & Spohn model, different initial mantle temperatures give rise to different time histories. Schubert's model varies χ , a crustal fractionation parameter (see text).

the model, we inject the volcanic gases directly into the atmosphere. The volcanic gases are distributed log-normally through the lower 20 km of the atmosphere (Smith et al., 2014; Zahnle et al., 2006, 2008). The ground-level mixing ratios are insensitive to the vertical distribution of the injected volcanic gases.

The composition of volcanic gases depends on the magmas that produce them, and thus varies according to the oxygen fugacity (fO_2), pressure at outgassing, and water content of the mantle. Gaillard et al. (2013) modeled martian magmas, varying the aforementioned parameters, to estimate volcanic gas compositions given in ppm wt%. These authors assume a melt temperature of 1300 °C, magmatic S content at 3500 ppm, and nominally 0.08 wt% CO_2 (0.02 wt% CO_2 for the most reduced mantles, i.e. IW). We calculate the outgassing rate of species A (mol_A) in moles s^{-1} according to:

$$mol_A = \frac{s_A k_{dg} V \rho}{w_A} \quad (4)$$

here, s_A is the weight fraction of species A given by Gaillard et al. (2013), k_{dg} is the fraction of the species outgassed (here it is unity following Gaillard et al., 2013), V is the volumetric rate of lava being extruded in $km^3 yr^{-1}$, ρ is the density of the lava (assumed to be basalt of $2.9 g cm^{-3}$ after Wignall (2001)), and w_A is the molecular weight of species A (Leavitt, 1982). The fluxes for each species are converted into photochemical model units of molecules $cm^{-2} s^{-1}$ and we vary V to simulate greater amounts of volcanism over time. We present the outgassing rates and ratios in Appendix C for the range of martian magma parameters.

The redox state and water content of martian magmas are uncertain. Consequently, we use the emitted volcanic volatile amounts over a range of fO_2 and water content from the outgassing model of Gaillard et al. (2013) to simulate the fluxes of volcanic species of erupted magmas. The redox state of the melt is defined by its fO_2 , which is represented by mantle mineral buffers. The fayalite-magnetite-quartz (FMQ) buffer is defined with an $fO_2 = 10^{-8.5}$ and is less reduced than the iron-wüstite (IW) buffer with $fO_2 = 10^{-11.9} \cong FMQ-3.5$. Estimates from martian meteorites suggest that the martian mantle has an fO_2 of FMQ-1 to FMQ-3 (Herd et al., 2002); to test this range, three buffers were used: FMQ-0.5, FMQ-1.4, and IW. Water content of the magmas is varied between dry melts with 0.01 wt% H_2O and wet melts with 0.4 wt% H_2O . The highest estimate of water content for Mars

is an upper limit of 1.8 wt% from martian basaltic meteorites (McSween et al., 2001), but this may represent the effect of cumulate processes (e.g. assimilation of drier crustal material) and not the composition of the melt (Gaillard et al., 2013), and so is broadly consistent with our upper value of 0.4 wt% H_2O . However, others have argued for a drier mantle (Wänke and Dreibus, 1994), consistent with our lower value. The pressure at outgassing is varied between 0.01 bar and 1 bar. We vary the volumetric rate of lava from 0.001 to $1 km^3 yr^{-1}$ to simulate ranges around the time-average of $0.17 km^3 yr^{-1}$ over the past 3.5 Ga.

As a first-order test, we only examine the necessary conditions required to switch the current martian atmosphere into an anoxic reducing regime. We assume that the gases are being emitted at depth and the outgassing pressure represents the lithostatic pressure of the melt rather than the atmospheric surface pressure. This implementation gives a good representation of how much volcanism it takes to reach anoxic and reducing conditions. As a sensitivity test, we ran the model with atmospheric pressure matching the outgassing pressure and used the corresponding temperature profile as modeled by Ramirez et al. (2014). However, with greater temperatures the absolute humidity increases, as expected from the results of Zahnle et al. (2008), and the atmosphere is overall reducing even with no volcanic activity because much CO is produced. An additional sensitivity test was done to include the outgassing of H_2O based on the Gaillard et al. (2013) values. However, we found that no significant changes occurred.

In our photochemical model, we quantify the redox state due to the influx of volcanic gases as follows. We define the net redox balance (pOx) of the atmosphere as (Zahnle et al., 2008)

$$pOx \approx 2pO_2 - pCO - pH_2 \quad (5)$$

where pO_2 , pCO , and pH_2 are the partial pressure of oxygen, carbon monoxide, and hydrogen respectively. Eq. (5) is an approximation based on the dominant oxidants and reductants in the atmosphere. This equation can be expanded to include all non-redox neutral species, but only the three terms shown dominate. Even when OCS (carbonyl sulfide) concentrations reach ppm levels in anoxic atmospheres, pCO dominates. Modern Mars has an oxidizing atmosphere with a net redox state of $pOx \approx 15 \mu bar$, which is an imbalance caused by photodissociation of water vapor and subsequent rapid escape of hydrogen to space that leaves oxygen behind. As the atmosphere switches to a reducing regime, the redox state given by pOx will shift through zero and then become negative. Once pOx is negative, the atmospheric redox becomes dominated by the reducing gases CO and H_2 , while O_2 becomes a trace gas. Thus, $pOx = 0$ defines a tipping point.

3. Results

We find that relatively small to moderate amounts of volcanic outgassing would have dramatically modified the past chemical composition and redox state of the martian atmosphere. Fig. 3 shows how modeled martian atmospheres respond to increasing amounts of volcanic outgassing with varying mantle parameters including redox state, water content, and pressure of outgassing. At low levels of volcanic magma flux (typically $< 10^{-3} km^3 yr^{-1}$), the model atmosphere is largely unaffected, and remains oxidizing and similar to modern-day Mars. As the magma flux is ramped up, larger amounts of reducing gases flux into the atmosphere and the available free atmospheric oxygen declines as reactions produce oxidized species (e.g. CO_2 , H_2O , SO_2).

In our simulations, reducing gases can reach abundances on the order of a few percent under plausible volcanic outgassing levels. The abundance of hydrogen, and the escape of hydrogen to space, also increases as volcanic input is ramped up. In particular, CO builds up to become a bulk constituent with a volume mixing

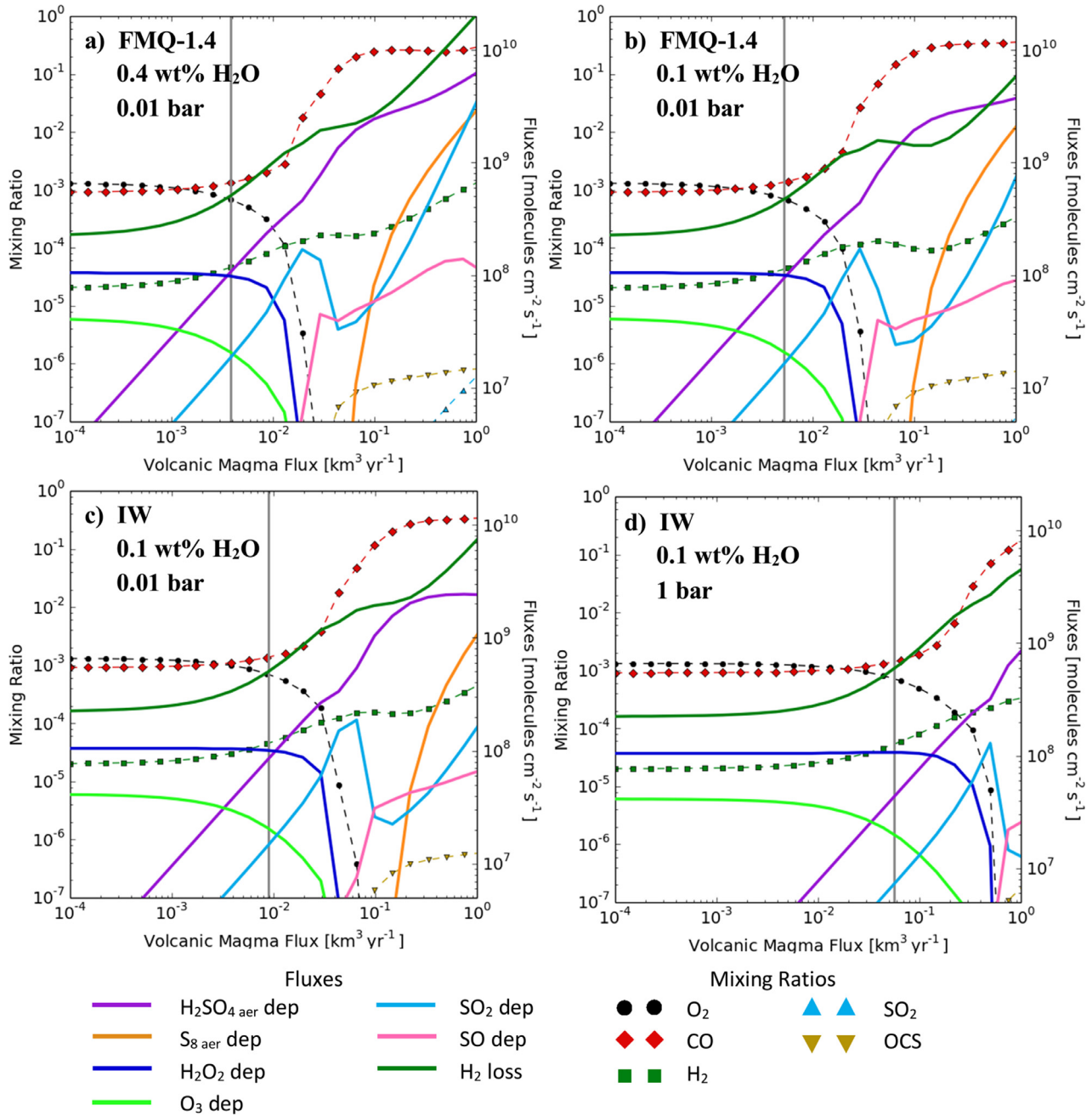


Fig. 3. Atmospheric response to steady-state volcanic outgassing from typical martian magmatic buffers. Symbols display the mixing ratios (mapped to left axes) and solid lines display species and aerosol (aer) surface deposition (dep) fluxes and atmospheric loss for H_2 (mapped to right axes). We used magma buffers to illustrate how a state of anoxia depends on the total amount of volcanic magma flux for each buffer. A vertical gray line shows the transition point between oxidizing and reducing conditions as dictated by Eq. (5). Plots *a* through *d* show the cumulative effects of changing each melt parameter; *b* is a drier melt, *c* is more reduced, and *d* is outgassed under higher pressures. Melts that are drier, more reduced, and under greater pressure take the greatest amount of volcanism to reach reducing conditions ($\sim 4 \times 10^{-3} \text{ km}^3 \text{ yr}^{-1}$ for *a* versus $\sim 6 \times 10^{-2} \text{ km}^3 \text{ yr}^{-1}$ for *d*).

ratio of $\sim 10\%$ or more. The main sink on CO is the hydroxyl radical, OH, which on Mars is derived from H_2O photolysis. These simulations assume a background atmosphere that is cold and dry, similar to the modern one, so CO does not have much of an OH sink and thus the volcanic gases build up, contributing to a highly reduced atmosphere. In a reduced state, there is negligible free oxygen and the atmosphere is anoxic.

Fig. 3a–d show the effects of varying each melt parameter. Decreasing f_{O_2} of the magma, or decreasing the magma's water content, have the counter-intuitive effect of making it more difficult to reach reducing anoxic conditions (requiring greater amounts of volcanic magma fluxes) because more sulfur stays in the melt, as

discussed below. Increases in the pressure of outgassing have a similar effect. Thus wet and more oxic melts at lower pressures allow the atmosphere to reach anoxia under lower volcanic fluxes than their reducing, dry, high-pressure counterparts.

The model also predicts that sulfur gases, such as SO_2 and the reduced form SO, would be likely to react directly with the surface, as the depositional fluxes of these gases build up to relatively high levels. As the atmospheres become anoxic, a shift occurs as more moles of S exit the atmosphere as elemental polysulfur than as sulfate. As this happens, a small ramp up in the sulfate production limits available sulfur and decreases in SO_2 and SO deposition occur around or below a volcanic magma flux rate of $\sim 0.1 \text{ km}^3 \text{ yr}^{-1}$

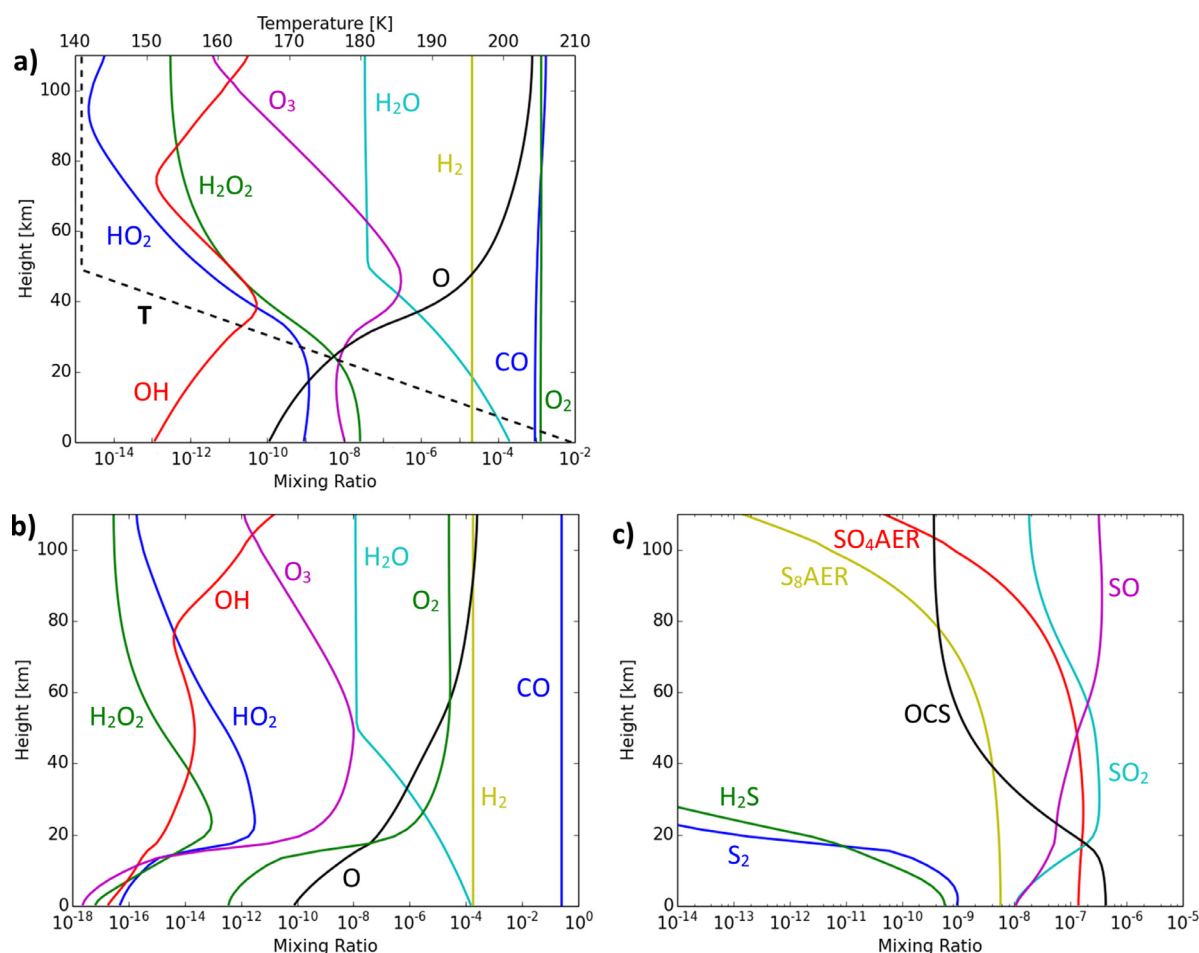


Fig. 4. Vertical mixing ratio profiles for modern and anoxic Mars. Temperature (T) is plotted as a dashed line. (a) C–O–H species for modeled modern Mars, (b) C–O–H species for anoxic Mars for the case of mantle buffer with FMQ-1.4, 0.4 wt% H₂O at 0.01 bar and magma flux of 0.15 km³ yr⁻¹ which is a good representation of typical modeled reducing and anoxic conditions (See Fig. 3a), (c) S species for anoxic Mars under the same conditions as b.

(Fig. 3a–c). In reducing atmospheres with high volcanic outgassing, SO₂ and OCS are able to build up levels approaching ~1 ppm.

We can quantify the shift to anoxic, reducing conditions using Eq. (5). Reducing conditions occur when the *pOx* shifts from positive (oxidizing) to negative (reducing) values. The *pOx* can shift from modern-day values of ~15 μbar to less than -700 μbar in anoxic atmospheres (e.g. >3 × 10⁻² km³ yr⁻¹ in Fig. 3a) primarily because of increased CO and lack of O₂ in the atmosphere. Regardless of the magma buffer used, all simulated atmospheres reached an anoxic reducing state within the modeled magmatic flux parameter space for magma production rates >0.14 km³ yr⁻¹.

Vertical mixing ratio profiles for various model atmospheres are plotted in Fig. 4. Even in highly reducing atmospheric conditions, the O₂ mixing ratio remains fairly large (~10 ppm) above the tropopause. The lower atmosphere is anoxic and reducing, while the upper atmosphere is less reducing, similar to models of a reducing atmosphere on the early Earth (Claire et al., 2014).

The chemistry of anoxic tropospheres produces elemental polysulfur, S₈, and sulfate, H₂SO₄ aerosols (see fluxes in Fig. 3). Sulfate aerosols readily form with even low volcanic fluxes and increase monotonically with volcanic flux. S₈ particles are only produced in large quantities once anoxic conditions are reached and elemental sulfur gases are no longer preferentially oxidized into sulfuric acid (see Fig. 1). Free elemental sulfur gases are also able to react with the abundant CO to form carbonyl sulfide (OCS), through the dominant net reactions:



This allows OCS to build up to the ppm level in reducing martian atmospheres.

It is instructive to integrate the deposition of sulfate over time for different volcanic outgassing histories because we can compare the integrated sulfate with estimates of the total sulfate inventory in martian soil and in light-toned layered deposits on Mars. The deposition rates of sulfate aerosols produced over Mars' history in model runs is shown in Fig. 5a, corresponding to the different crustal production rate models shown earlier in Fig. 2. Rates of SO₂, S₈, and H₂S deposition are also shown in Fig. 5. Deposition rates for SO and S₂ molecules are minor and always less than 0.02 Tmol yr⁻¹ (teramoles = 10¹² moles). Sulfate depositional fluxes were integrated over the entirety of the volcanic history for both an oxidizing wet magma buffer (FMQ-0.5, 0.4 wt% H₂O, 0.01 bar) and a reducing dry magma buffer (IW, 0.01 wt% H₂O, 1 bar) to cover the range of how much sulfate can be produced. These total integrated amounts of sulfate and elemental polysulfur deposition over the past 3.5 Gyr are given in Table 1. For most volcanic models, the total amount of sulfate ranges from ~5 × 10⁹ Tmol for sulfur-producing mantles and high volcanism to ~2 × 10⁶ Tmol for sulfur-retaining mantles and low total volcanism. For comparison, estimates of the total amount of sulfur in the sulfate sedimentary rock reserves on Mars is of order 10⁶ Tmol (Catling, 2014; Michalski and Niles, 2012).

In low volcanism models with reduced dry melts, there is no S₈ deposition but in high total volcanism models with oxidized wet

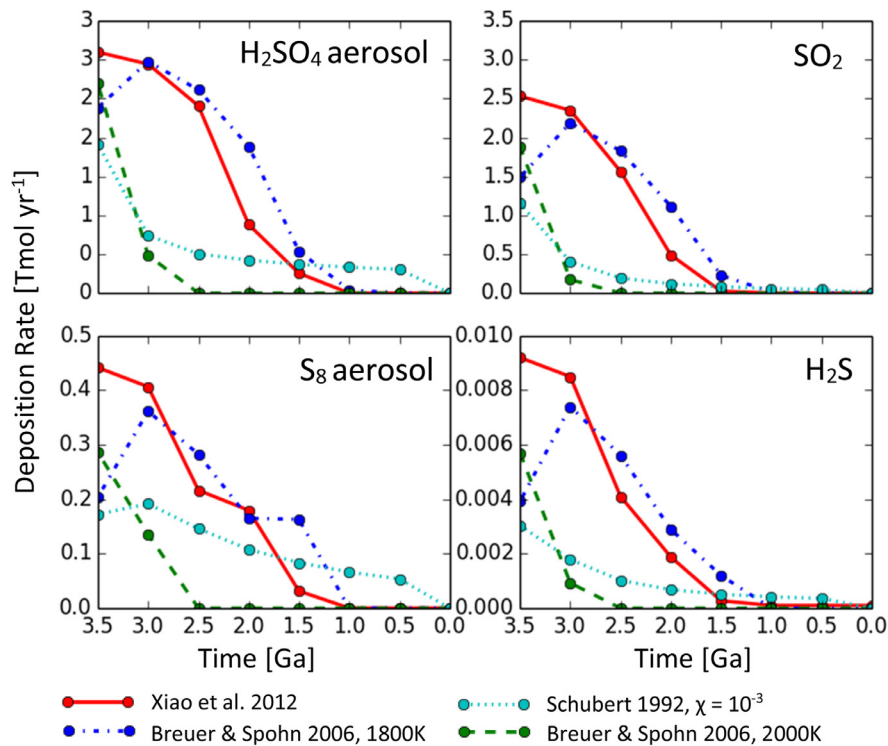


Fig. 5. Deposition rates based on varying crustal production models (see Fig. 2; χ is a crustal fractionation parameter – see text). Total amounts of sulfate deposited are given in Table 1. Deposition rates for SO and S₂ are always less than 0.02 Tmol yr⁻¹.

Table 1

Modeled approximate total amounts of sulfate deposited (dep.) over the 3.5–0 Gyr volcanic history of Mars for different crustal production rates and mantle buffers of oxygen fugacity: FMQ-0.5 (Fayalite-Magnetite-Quartz; with 0.4 wt% H₂O and 0.01 bar outgassing pressure) and IW (Iron-Wüstite; with 0.01 wt% H₂O and 1 bar outgassing pressure). S content of the magma is 3500 ppm. The total amount of each sulfur aerosol deposition is given in teramoles (1 Tmol = 10¹² mol). In Schubert's models, χ is an assumed crustal fractionation parameter (see text).

Reference for crustal production model	Key crustal production model parameter	Sulfate Dep. FMQ-0.5 (Tmol)	Sulfate Dep. IW (Tmol)	S ₈ Dep. FMQ-0.5 (Tmol)	S ₈ Dep. IW (Tmol)
Xiao et al. (2012)	Initial mantle temp. = 1900 K	4.0 × 10 ⁹	9.8 × 10 ⁶	5.2 × 10 ⁸	2.3 × 10 ⁻⁸
Breuer and Spohn (2006)	Initial mantle temp. = 1800 K	4.6 × 10 ⁹	1.1 × 10 ⁷	5.3 × 10 ⁸	1.4 × 10 ⁻⁸
Breuer and Spohn (2006)	Initial mantle temp. = 2000 K with primordial crust	9.1 × 10 ⁸	2.3 × 10 ⁶	1.4 × 10 ⁸	2.1 × 10 ⁻⁹
Schubert et al. (1992)	$\chi = 10^{-3}$	1.7 × 10 ⁹	4.7 × 10 ⁶	3.5 × 10 ⁸	Negligible

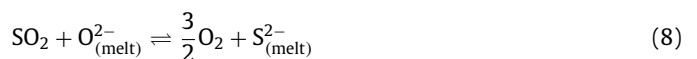
melts total S₈ deposition ranges up to $\sim 5 \times 10^8$ Tmol of S₈. The difference is discussed below. Additionally, because volcanic activity is not continuous, the majority of the sulfur aerosol production and precipitation will occur during discrete highly volcanic epochs. There will be a bias for S to exit as S₈ during the intense episodes of volcanism compared to the average conditions modeled here.

4. Discussion

4.1. Consequences of volcanism

The range of mantle buffers from Gaillard et al. (2013) (depending on magma water content, pressure of outgassing, and oxygen fugacity (fO_2)) all predict volcanic outgassing where the redox state of the atmosphere switches from oxidizing to reducing for crustal production rates $> 0.14 \text{ km}^3 \text{ yr}^{-1}$. Such rates of volcanic activity are relatively low compared to typical estimates for past Mars (Fig. 2). Water content and mantle fO_2 have the greatest impact on the amount of volcanic flux needed for an anoxic atmosphere. As mentioned earlier, we obtain the counterintuitive result that the more reducing conditions of the IW melts require

greater total volcanic flux to produce a reducing atmosphere. These effects are predominantly at higher outgassing pressures and in drier melts. While the volcanic emissions from reducing magmas are composed of a higher percentage of reducing gases than the more oxic buffers, they can require up to an order of magnitude greater amount of volcanic production to reach the redox switch. This is because sulfur is more stable in the melt at lower fO_2 (Fincham and Richardson, 1954; O'Neill and Mavrogenes, 2002). The following equilibrium controls sulfur in the melt:



Following Le Châtelier's Principle, decreasing fO_2 (on the right side of Eq. (8)) causes an increase in melt sulfide while simultaneously decreasing the emitted sulfur dioxide. Higher pressures act to make the sulfur more siderophile (iron-loving) in the melt, thus the sulfur prefers to be in the form of metal sulfides than as a gas (Li and Agee, 1996). The effect of high water content on outgassed sulfur is predominantly the result of dilution effects – the gas-phase species are dominated by water and thus yield relatively sulfur-poor gases (Gaillard and Scaillet, 2009), given the fixed outgassing pressure. Dry melts retain more sulfur in the

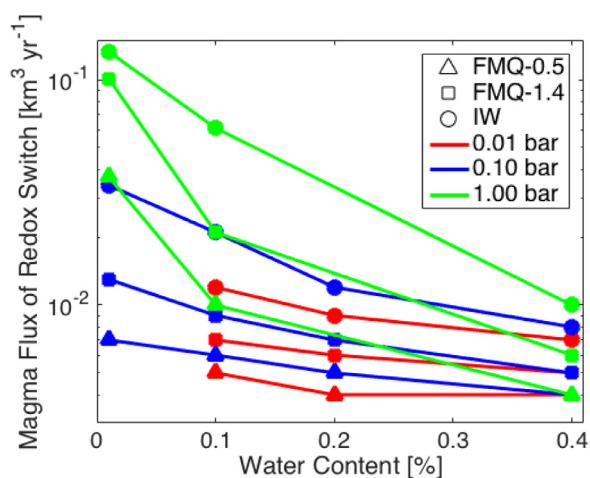


Fig. 6. Plot showing crustal production flux (in $\text{km}^3 \text{yr}^{-1}$) (associated with volcanic outgassing) needed to reach a reducing atmosphere ($p\text{O}_x < 0$) as a function of magma water content (along x-axis), outgassing pressure (color), and redox state of the magma (symbols). Drier, more reducing magmas take the greatest amount of volcanic activity to switch the redox of the martian atmosphere.

melt, caused by partitioning the sulfur in the melt, but produce more sulfur-rich gases. With less sulfur outgassed in the low $f\text{O}_2$ regimes, a major sink for atmospheric oxygen is lost. In sulfur-rich systems, outgassed sulfur readily reacts with oxidizing species, first forming intermediate products, e.g. SO_3 , and eventually forming sulfate aerosols (H_2SO_4). The sulfate falls out of the atmosphere.

Over a large parameter space, only moderate amounts of volcanism are required to switch the atmosphere's redox state from oxidizing to reducing. Given plausible $f\text{O}_2$ and water-content constraints on martian melts, magmatism on the order of 0.01–0.14 $\text{km}^3 \text{yr}^{-1}$ (Fig. 6) is enough to eliminate free oxygen from a past martian atmosphere that is similar to today's. These values are well within the range of estimated volcanic activity on Mars in the past. Photogeological studies estimate an average magma extrusion rate of 0.17 $\text{km}^3 \text{yr}^{-1}$ over the past 3.8 Gyr, and crustal production models estimate the rate to be between 0–4 $\text{km}^3 \text{yr}^{-1}$ over the past 3.5 Gyr (Fig. 2).

Given that the moderate amount of volcanism required is well within estimated values from the Late Hesperian to Middle Amazonian, our results suggest that the past martian atmosphere should have had episodes of mildly to strongly reducing atmospheres throughout most of Mars' early Amazonian history, ~ 3.5 –1.0 Ga. However, volcanic eruptions are well known for being episodic, so activity was not continuous. Consequently, the atmosphere should have had periods of oxidizing atmospheres during volcanic quiescence, and today's atmosphere is such a state.

4.2. Implications for Habitability

The origin of life requires the presence of prebiotic organic chemical compounds, which are most efficiently produced in reducing conditions (Orgel, 1998). Highly reducing atmospheres, such as those with high concentrations of CH_4 or ammonia (NH_3), can synthesize organic molecules, such as amino acids (Miller, 1953, 1955) or precursors of nucleobases (i.e. hydrogen cyanide (HCN) for purines and cyanoacetylene and urea for pyrimidines) (Miller, 1986). Even weakly reducing atmospheres can build such compounds (Abelson, 1966; Pinto et al., 1980; Tian et al., 2005; Zahnle, 1986). The high abundance of OCS in anoxic atmospheres could also have polymerized accumulated amino acids to form peptides (Johnson et al., 2008a; Leman et al., 2004).

The most reducing of our model atmospheres are CO-dominated, and these are well documented to efficiently produce

organic prebiotic compounds via the photolysis of H_2O and CO. Carbon monoxide can also be used directly as a substrate for prebiotic chemistry (Huber and Wächtershauser, 1998). Acetic and formic acids, along with a variety of alcohols, aldehydes, and acetone can easily be built in these atmospheres with relatively high quantum yields (Bar-Nun and Chang, 1983; Bar-Nun and Hartman, 1978; Hubbard et al., 1973; Miyakawa et al., 2002). All of our modeled atmospheres eventually became weakly to highly reducing with realistic amounts of volcanism. Consequently, past, volcanically active Mars may have been more suitable to the genesis of prebiotic chemistry.

Abundant CO in the atmosphere also provides a source of free energy for potential life to utilize. A dominant pathway for CO metabolisms is as follows:



This pathway occurs in organisms on Earth and is an efficient way of extracting energy from the atmosphere if liquid water is present (Kharecha et al., 2005; Ragsdale, 2004).

Abundant CO also enables significant quantities of OCS to form. OCS is a greenhouse gas which has been hypothesized in warming scenarios for the early Earth (Byrne and Goldblatt, 2014; Ueno et al., 2009), but the lack of CO combined with more vigorous photolysis by the young Sun prevents OCS concentrations from growing large in plausible early Earth scenarios (Domagal-Goldman et al., 2011). The primary sink of OCS is in sulfate aerosols, so it is likely to have a similar net radiative effect as SO_2 , where cooling from aerosols is important. On the modern Earth, the negative forcing from stratospheric sulfate aerosols derived from OCS photochemistry approximately cancels the positive radiative forcing from OCS acting as a greenhouse gas (Brühl et al., 2012).

4.3. Potentially observable consequences of anoxia

Given past volcanic activity and expected reducing anoxic conditions, there should be geochemical features associated with such atmospheric conditions, particularly the deposition of sulfur to the surface. The most obvious observable is the large amount of sulfur-bearing aerosols deposited directly on the surface as both H_2SO_4 and S_8 during high volcanism. Sulfate minerals have readily been observed both in situ and remotely largely in the form of jarosite ($\text{KFe}^{3+}(\text{SO}_4)_2(\text{OH})_6$), kieserite ($\text{MgSO}_4 \cdot \text{H}_2\text{O}$), and gypsum ($\text{CaSO}_4 \cdot 2\text{H}_2\text{O}$) (Murchie et al., 2009; Squyres et al., 2004). Elemental polysulfur has yet to be discovered in any martian rocks. Possibly, S_8 is subject to post-depositional oxidation or burial. *In situ* detection from landers would need to account for S_8 breaking up into reactive fragments during pyrolysis experiments. If found, S_8 would indicate periods when volcanism was relatively high and conditions were almost certainly reducing and anoxic.

Detection of S_8 could be done using the instruments on the Mars Science Laboratory (MSL) or the future Mars 2020 rover mission. When heated, vapor phase S_8 dominates but will also break into smaller chains at higher temperatures – typically S_2 but also S, S_4 , and S_6 . From the mass to charge ratios, S_2 and S could be confused for more common species (e.g. SO_2 and O_2 respectively) whereas S_4 and S_6 would have fewer interferences. During pyrolysis, vapor S may react with released H_2O to form SO_2 and other sulfides. Elemental sulfur has not yet been found on Mars, but SO_2 and H_2S have, which are interpreted to be the thermal decomposition of iron sulfates or calcium sulfites but are consistent with sulfur-bearing amorphous phases (McAdam et al., 2014).

The lower negligible estimate for total S_8 production comes from dry reduced melts in a low total volcanism model. These atmospheres are not able to reach anoxic conditions and therefore unable to initiate S_8 aerosol production. However, these models

all represent continuous average volcanism and there may be brief periods where enough volcanism occurred to shift the atmosphere anoxic and some non-negligible S_8 could be deposited.

Martian elemental sulfur and sulfate produced in an anoxic troposphere should produce mass-independent fractionation (MIF) sulfur isotopes, although direct interrogation of this record would likely require sample return. The magnitude and sign of MIF sulfur depend on the incident radiation field, the concentration of sulfur gases, their respective depositional fluxes, as well as on the concentrations of absorbing gases (such as OCS) in the atmosphere above the region of SO_2 photolysis (Claire et al., 2014). These elements would combine to produce sulfur MIF signatures distinct to those seen on Earth.

The total amount of sulfate estimated to be on the surface of Mars today, $\sim 10^6$ Tmol (Catling, 2014; Michalski and Niles, 2012), is of the same order of magnitude of the model-predicted amount for the most sulfur-retaining melts over low total volcanism models. However, data from sulfur isotope MIF in martian meteorites suggests that some of the sulfur assimilates into magmatic processes and some sulfate is reduced to sulfide (Franz et al., 2014). This converted sulfur provides a subsurface reservoir of sulfur that may explain loss of sulfur in the case of large sulfate deposition. Realistically, Mars probably either experienced intermittent periods of volcanism (producing less sulfates) or there are greater unseen reserves of sulfates buried. Sulfate may also be hidden in cements of sandstones, which may not have been fully accounted for in published inventories.

Anoxic reducing conditions could also have affected the minerals formed on the surface of Mars in the past. One possible indicator volatile is carbonyl, derived from CO. The two most commonly found carbonyls, iron pentacarbonyl ($Fe(CO)_5$) and nickel tetracarbonyl ($Ni(CO)_4$), readily form in reducing CO-rich environments – such as those in the end state of our models. While iron pentacarbonyl should exist in the Earth's mantle (Wetzel et al., 2013), and presumably Mars' as well, areas of enrichment relative to the mantle may indicate more reducing conditions. Additionally, siderite ($FeCO_3$) is a good tracer for anoxia (Catling, 1999) and reducing conditions (Hausrath and Olsen, 2013). Siderite generally forms from acidic waters which allows soluble ferrous iron (Fe^{2+}) to exist in solution. Acidic waters are common in CO_2 -rich environments, as expected on early Mars and during periods of ephemeral liquid surface waters. In oxic atmospheric conditions, O_2 dissolved in the water would rapidly oxidize the ferrous iron into minerals that can end up as hematite (Fe_2O_3). In anoxic atmospheres, the ferrous iron can form siderite. Due to lowest solubility amongst the carbonates, siderite will be the first to precipitate out, followed by magnesium carbonate. Siderite has been found on Mars at the Comanche site in Gusev Crater (Morris et al., 2010; Ruff et al., 2014) and possible ancient layered carbonates excavated in impact craters (Michalski and Niles, 2010). These siderite deposits may be evidence of such anoxic conditions, although they could also be representative of local hydrothermal activity (Ehlmann et al., 2008).

Clay minerals, especially phyllosilicates, have been mapped on Mars from orbital spectrometers (Bibring et al., 2005; Ehlmann et al., 2013; Poulet et al., 2005) and the predicted anoxic reducing conditions should have affected the types of clays forming on early Mars (Chemtob et al., 2015; Peretyazhko et al., 2016). The highly reducing conditions at the surface would, by definition, create an environment with negative Eh, which allows Fe^{2+} to be soluble. In Eh-pH conditions that favor ferrous iron, octahedral clays will form, such as saponites and talc (Velde, 1992). The most common clay to form with abundant Fe^{2+} and low Eh is berthierine, a trioctahedral Fe-rich clay mineral of the kaolinite-serpentine group with the general formula $(Fe^{2+}, Fe^{3+}, Al, Mg)_{2-3}(Si, Al)_2O_5(OH)_4$. However, berthierine can form in both oxidizing and reducing

conditions (positive and negative Eh respectively) and therefore cannot be a sole indicator mineral of reducing anoxic conditions (Chevrier et al., 2007).

In addition to the presence of berthierine, indicating acidic and/or reducing conditions, the absence of nontronite, an Fe^{3+} -rich smectite that requires highly oxidizing conditions to form (Chevrier et al., 2007), may provide evidence of reducing conditions. Levels of pH are similarly important in the formation of both nontronite and berthierine: the former is favored by neutral to weakly alkaline conditions and the latter by alkaline solutions. While paleo-pH levels are unknown for early Mars, the high partial pressures of CO_2 (and to a lesser extent SO_2) may have led to more acidic conditions, which would lead to aqueous Fe^{2+} and the formation of minerals such as pyrite (FeS_2). However, some aqueous environments would be buffered by basaltic minerals to higher pH. Overall, the reducing and anoxic conditions of early Mars should have favored Fe-rich clays (Harder, 1978) and Fe/Mg smectite secondary minerals (Dehouck et al., 2016).

5. Conclusions

We used a 1-dimensional photochemical model to calculate the composition and redox state for past martian atmospheres (~ 3.5 Gyr to present) for plausible levels and compositions of volcanic outgassing. The results suggest the following conclusions:

- The atmospheric redox state can rapidly shift from oxidizing to reducing conditions at levels of extrusive volcanism $> 0.14 \text{ km}^3 \text{ yr}^{-1}$ under a range of reasonable melt parameters and magmatic oxygen fugacity, water content, and outgassing pressure constraints. This shift is driven primarily by the release of large quantities of reducing gases (e.g. CO and H_2) and the formation of sulfate aerosols which act as a large sink of oxygen.
- When Mars was volcanically active, it should have produced a considerable flux of sulfur-bearing aerosols. In oxidizing and transitional-to-anoxic atmospheres, sulfate aerosols are the most important aerosols with $\sim 10^6$ – 10^9 Tmol of sulfate being deposited over the volcanic outgassing history since 3.5 Ga. Reducing conditions also allow the deposition of elemental polysulfur aerosols ranging from $\sim 10^{-8}$ Tmol S_8 to $\sim 10^8$ Tmol S_8 , when rates are non-negligible. S_8 deposition onto the surface increases in more reducing atmospheres. The smallest deposition occurs at IW oxygen fugacity when S stays in the melt. Detection of elemental polysulfur or a distinct sulfur MIF isotopic signature would indicate past reducing atmospheres.
- Reducing anoxic environments should lead to the formation of minerals that are favored by low-Eh and/or contain ferrous iron (Fe^{2+}). Trioctahedral Fe-rich clays, such as berthierine, should be favored, and the absence of clays that only form under high Eh (e.g. nontronite) can indicate reducing conditions. The formation of minerals such as siderite, nickel carbonyl, and pyrite may also be indicative of anoxia, especially if found in bedded deposits that were subaerial.
- The formation of prebiotic chemical compounds is possible in anoxic and reducing atmospheres expected from a volcanically active early Mars. The atmospheric formation of organics, such as amino acids, may have created conditions making a martian *de novo* origin of life possible.

Acknowledgments

This work was supported by NNX10AN67G grant from NASA's Mars Fundamental Research Program awarded to DCC. We also thank the two anonymous reviewers who improved the clarity of the paper.

Appendix A. Photochemical reactions involving sulfur species

#	Reactants ^a		Products	Rate [cm ³ s ⁻¹] or [cm ⁶ s ⁻¹] ^b	Reference
1	SO + O ₂	→	O + SO ₂	$2.4 \times 10^{-13} e^{-2370/T}$	Sander et al. (2006)
2	SO + O	→	SO ₂	$6.0 \times 10^{-31} \times den$	Sander et al. (2006)
3	SO + OH	→	SO ₂ + H	8.6×10^{-11}	Sander et al. (2006)
4	SO + NO ₂	→	SO ₂ + NO	1.4×10^{-11}	Sander et al. (2006)
5	SO + O ₃	→	SO ₂ + O ₂	$4.5 \times 10^{-12} e^{-1170/T}$	Atkinson et al. (2004)
6	SO + SO	→	SO ₂ + S	3.5×10^{-15}	Martinez and Herron (1983)
7	SO + HCO	→	HSO + CO	$5.6 \times 10^{-12} (T/298)^{-0.4}$	Kasting (1990)
8	SO + H + M	→	HSO + M	$k_0 = 5.7 \times 10^{-32} (T/300)^{-1.6}$ $k_\infty = 7.5 \times 10^{-11}$	Kasting (1990)
9	SO + HO ₂	→	SO ₂ + OH	2.8×10^{-11}	Kasting (1990) ^c
10	SO ₂ + OH + M	→	HSO ₃ + M	$k_0 = 3.0 \times 10^{-31} (T/300)^{3.3}$ $k_\infty = 1.5 \times 10^{-12}$	Sander et al. (2006)
11	SO ₂ + O + M	→	SO ₃ + M	$k_0 = 1.3 \times 10^{-33} (T/300)^{-3.6}$ $k_\infty = 1.5 \times 10^{-11}$	Sander et al. (2006)
12	SO ₂ + HO ₂	→	SO ₃ + OH	8.6×10^{-16}	Lloyd (1974) ^c
13	SO ₃ + H ₂ O	→	H ₂ SO ₄	1.2×10^{-15}	Sander et al. (2006)
14	SO ₃ + SO	→	SO ₂ + SO ₂	2.0×10^{-15}	Chung et al. (1975)
15	HSO + OH	→	H ₂ O + SO	5.2×10^{-12}	Sander et al. (2006)
16	HSO + H	→	HS + OH	7.3×10^{-11}	Sander et al. (2006)
17	HSO + H	→	H ₂ + SO	6.5×10^{-12}	Sander et al. (2006)
18	HSO + HS	→	H ₂ S + SO	1.0×10^{-12}	Kasting (1990)
19	HSO + O	→	OH + SO	$3.0 \times 10^{-11} e^{-200/T}$	Kasting (1990)
20	HSO + S	→	HS + SO	1.0×10^{-11}	Kasting (1990)
21	HSO + NO	→	HNO + SO	1.0×10^{-15}	Atkinson et al. (2004) ^c
22	HSO ₃ + O ₂	→	HO ₂ + SO ₃	$1.3 \times 10^{-12} e^{-330/T}$	Sander et al. (2006)
23	HSO ₃ + H	→	H ₂ + SO ₃	1.0×10^{-11}	Kasting (1990) ^c
24	HSO ₃ + O	→	OH + SO ₃	1.0×10^{-11}	Kasting (1990) ^c
25	HSO ₃ + OH	→	H ₂ O + SO ₃	1.0×10^{-11}	Kasting (1990) ^c
26	H ₂ S + OH	→	H ₂ O + HS	$6.1 \times 10^{-12} e^{-81/T}$	Atkinson et al. (2004)
27	H ₂ S + H	→	H ₂ + HS	$1.5 \times 10^{-11} e^{-855/T}$	Schofield (1973)
28	H ₂ S + O	→	OH + HS	$9.2 \times 10^{-12} e^{-1800/T}$	DeMore et al. (1997)
29	H ₂ S + S	→	HS + HS	$1.4 \times 10^{-10} e^{-3720/T}$	Shiina et al. (1996) ^c
30	H ₂ S + CH ₃	→	HS + CH ₄	$2.1 \times 10^{-13} e^{-1160/T}$	Perrin et al. (1988) ^c
31	HS + O	→	H + SO	1.6×10^{-10}	Sander et al. (2006)
32	HS + OH	→	S + H ₂ O	$4.0 \times 10^{-12} e^{-240/T}$	Zahnle et al. (2016) ^c
33	HS + HO ₂	→	H ₂ S + O ₂	1.0×10^{-11}	Stachnik and Molina (1987)
34	HS + HS	→	H ₂ S + S	1.5×10^{-11}	Schofield (1973)
35	HS + HS	→	S ₂ + H ₂	$1.3 \times 10^{-11} e^{-20,600/T}$	Zahnle et al. (2016) ^c
36	HS + HCO	→	H ₂ S + CO	5.0×10^{-11}	Kasting (1990)
37	HS + H	→	H ₂ + S	3.0×10^{-11}	Schofield (1973)
38	HS + H + M	→	H ₂ S + M	$1.4 \times 10^{-31} (T/298)^{-2.5} e^{500/T}$	Zahnle et al. (2016) ^c
39	HS + S	→	H + S ₂	4.0×10^{-11}	Schofield (1973)
40	HS + O	→	S + OH	$1.7 \times 10^{-11} (T/298)^{0.67} e^{-956/T}$	Schofield (1973) ^c
41	HS + O ₂	→	SO + OH	4.0×10^{-19}	Sander et al. (2006) ^c
42	HS + O ₃	→	HSO + O ₂	$9.0 \times 10^{-12} e^{-280/T}$	Sander et al. (2006)
43	HS + NO ₂	→	HSO + NO	$2.9 \times 10^{-11} e^{240/T}$	Sander et al. (2006)
44	HS + CO	→	OCS + H	$4.2 \times 10^{-14} e^{-7660/T}$	Kurbanov and Mamedov (1995)
45	HS + CH ₃	→	S + CH ₄	$4.0 \times 10^{-11} e^{-500/T}$	Shum and Benson (1985) ^c
46	HS + CH ₄	→	CH ₃ + H ₂ S	3.0×10^{-31}	Kerr and Trotman-Dickenson (1957) ^c
47	S + O ₂	→	SO + O	2.3×10^{-12}	Sander et al. (2006)
48	S + OH	→	SO + H	6.6×10^{-11}	DeMore et al. (1997)
49	S + HCO	→	HS + CO	6.0×10^{-11}	Moses et al. (1995)
50	S + HO ₂	→	HS + O ₂	1.5×10^{-11}	Kasting (1990)
51	S + HO ₂	→	SO + OH	1.5×10^{-11}	Kasting (1990)
52	S + CO ₂	→	SO + CO	1.0×10^{-20}	Yung and Demore (1982) ^c
53	S + H ₂	→	H ₂ S	$1.4 \times 10^{-31} (T/298)^{-1.9} e^{-8140/T}$	Zahnle et al. (2016) ^c
54	S + S	→	S ₂	$2.0 \times 10^{-33} e^{206/T} \times den$	Du et al. (2008) ^d
55	S + S ₂	→	S ₃	$2.8 \times 10^{-32} \times den$	Kasting (1990) ^d
56	S + S ₃	→	S ₄	$2.8 \times 10^{-31} \times den$	Kasting (1990) ^d
57	S + O ₃	→	SO + O ₂	1.2×10^{-11}	Sander et al. (2006)
58	S + CO	→	OCS	$6.5 \times 10^{-33} e^{-2180/T} \times den$	Domagal-Goldman et al. (2011) ^c
59	S + HCO	→	OCS + H	6.0×10^{-11}	Moses et al. (1995) ^c
60	S + S ₃	→	S ₂ + S ₂	4.0×10^{-11}	Zahnle et al. (2016)
61	S ₂ + O	→	S + SO	1.1×10^{-11}	Hills et al. (1987)
62	S ₂ + S ₂	→	S ₄	$2.8 \times 10^{-31} \times den$	Baulch et al. (1976) ^d
63	S ₃ + H	→	HS + S ₂	$5.0 \times 10^{-11} e^{-500/T}$	Zahnle et al. (2016) ^c
64	S ₃ + O	→	S ₂ + SO	$2.0 \times 10^{-11} e^{-500/T}$	Moses et al. (1995) ^c
65	S ₃ + CO	→	S ₂ + OCS	$1.0 \times 10^{-11} e^{-10,000/T}$	Zahnle et al. (2016) ^c
66	S ₄ + S ₄	→	S ₈	$7.0 \times 10^{-30} (T/298)^{-2.0} \times den$	Zahnle et al. (2016) ^d
67	S ₄ + H	→	S ₃ + HS	$5.0 \times 10^{-11} e^{-500/T}$	Zahnle et al. (2016) ^c

(continued on next page)

#	Reactants ^a		Products	Rate [cm ³ s ⁻¹] or [cm ⁶ s ⁻¹] ^b	Reference
68	S ₄ + O	→	S ₃ + SO	2.0 × 10 ⁻¹¹ e ^{-500/T}	Moses et al. (1995) ^c
69	¹ SO ₂ + O ₂	→	SO ₃ + O	1.0 × 10 ⁻¹⁶	Turco et al. (1982)
70	¹ SO ₂ + SO ₂	→	SO ₃ + SO	4.0 × 10 ⁻¹²	Turco et al. (1982)
71	³ SO ₂ + SO ₂	→	SO ₃ + SO	7.0 × 10 ⁻¹⁴	Turco et al. (1982)
72	OCS + O	→	CO + SO	7.8 × 10 ⁻¹¹ e ^{-2620/T}	Singleton and Cvetanovic (1988)
73	OCS + O	→	S + CO ₂	8.3 × 10 ⁻¹¹ e ^{-5530/T}	Singleton and Cvetanovic (1988)
74	OCS + H	→	CO + HS	9.1 × 10 ⁻¹² e ^{-1940/T}	Lee et al. (1977) ^c
75	OCS + OH	→	CO ₂ + HS	1.1 × 10 ⁻¹³ e ^{-1200/T}	Atkinson et al. (2004)
76	OCS + S	→	OCS ₂	8.3 × 10 ⁻³³ × <i>den</i>	Basco and Pearson (1967)
77	OCS + S	→	CO + S ₂	1.5 × 10 ⁻¹⁰ e ^{-1830/T}	Schofield (1973) ^c
78	OCS ₂ + S	→	OCS + S ₂	2.0 × 10 ⁻¹¹	Zahnle et al. (2006)
79	OCS ₂ + CO	→	2 OCS	3.0 × 10 ⁻¹²	Zahnle et al. (2006)
<i>Photolysis reactions^e</i>					
80	SO + hν	→	S + O	1.32 × 10 ⁻⁴	
81	H ₂ S + hν	→	HS + H	7.89 × 10 ⁻⁵	
82	S ₂ + hν	→	S + S	3.18 × 10 ⁻⁴	
83	S ₃ + hν	→	S ₂ + S	3.18 × 10 ⁻⁴	
84	S ₄ + hν	→	S ₂ + S ₂	3.18 × 10 ⁻⁴	
85	S ₈ + hν	→	S ₄ + S ₄	1.93 × 10 ⁻⁵	
86	SO ₃ + hν	→	SO ₂ + O	1.20 × 10 ⁻⁵	
87	SO ₂ + hν	→	SO + O	4.94 × 10 ⁻⁵	
88	SO ₂ + hν	→	¹ SO ₂	5.17 × 10 ⁻⁴	
89	SO ₂ + hν	→	³ SO ₂	3.11 × 10 ⁻⁷	
90	HSO + hν	→	HS + O	1.76 × 10 ⁻⁴	
91	OCS + hν	→	CO + S	6.89 × 10 ⁻⁶	
92	¹ SO ₂ + hν	→	³ SO ₂	1.0 × 10 ⁻¹²	Turco et al. (1982) ^f
93	¹ SO ₂ + hν	→	SO ₂	1.0 × 10 ⁻¹¹	Turco et al. (1982) ^f
94	¹ SO ₂ + hν	→	³ SO ₂ + hν	1.5 × 10 ⁺³	Turco et al. (1982) ^f
95	¹ SO ₂ + hν	→	SO ₂ + hν	2.2 × 10 ⁺⁴	Turco et al. (1982) ^f
96	³ SO ₂ + hν	→	SO ₂	1.5 × 10 ⁻¹³	Turco et al. (1982) ^f
97	³ SO ₂ + hν	→	SO ₂ + hν	1.1 × 10 ⁺³	Turco et al. (1982) ^f

^a M refers to the third body species (typically CO₂ for Mars).

^b *den* refers to the background density [cm⁻³] and T refers to the temperature [K]. *k*₀ is the low-density limiting rate constant and *k*_∞ is the high-density limiting rate constant for termolecular reactions [cm⁶ s⁻¹].

^c Added reactions that were not included in the previous versions of this model, Catling et al. (2010) and Smith et al. (2014).

^d These reactions have a minimum reaction rate of 5.0 × 10⁻¹¹ cm³ s⁻¹, which are generally consistent with those of Moses et al. (2002) and Yung et al. (2009).

^e Photolysis rates [s⁻¹] are evaluated at the top of the atmosphere subject for a 50° slant path, and reduced by a factor of 2 to account for the diurnal cycle. Absorption cross sections were obtained from JPL-11 (Sander et al. 2011).

^f These reaction rate constants [cm³ s⁻¹] are for the photolysis reactions modeled as two-body reactions.

Appendix A References

- Atkinson, R., et al., 2004. Evaluated kinetic and photochemical data for atmospheric chemistry: Volume I-gas phase reactions of O x, HO x, NO x and SO x species. *Atmospheric chemistry and physics*, 4, 1461–1738.
- Basco, N., Pearson, A., 1967. Reactions of sulphur atoms in presence of carbon disulphide, carbonyl sulphide and nitric oxide. *Transactions of the Faraday Society*, 63, 2684–2694.
- Baulch, D. L., 1972. Evaluated kinetic data for high temperature reactions. CRC Press, 1.
- Chung, K., Calvert, J. G., Bottenheim, J. W., 1975. The photochemistry of sulfur dioxide excited within its first allowed band (3130 Å) and the “forbidden” band (3700–4000 Å). *International Journal of Chemical Kinetics*, 7, 161–182.
- DeMore, W. B., et al., 1997. Chemical Kinetics and Photochemical Data for Use in Stratospheric Modeling. Evaluation No. 12.
- Domagal-Goldman, S. D., Meadows, V. S., Claire, M. W., Kasting, J. F., 2011. Using biogenic sulfur gases as remotely detectable biosignatures on anoxic planets. *Astrobiology*, 11, 419–441.
- Du, S., Francisco, J. S., Shepler, B. C., Peterson, K. A., 2008. Determination of the rate constant for sulfur recombination by quasiclassical trajectory calculations. *The Journal of chemical physics*, 128, 204,306.
- Hills, A. J., Cicerone, R. J., Calvert, J. G., Birks, J. W., 1987. Kinetics of the reactions of diatomic sulfur with atomic oxygen, molecular oxygen, ozone, nitrous oxide, nitric oxide, and nitrogen dioxide. *Journal of Physical Chemistry*, 91, 1199–1204.
- Kasting, J. F., 1990. Bolide impacts and the oxidation state of carbon in the Earth's early atmosphere. *Origins of Life and Evolution of the Biosphere*, 20, 199–231.
- Kerr, J., Trotman-Dickenson, A., 1957. The reactions of methyl radicals with thiols. *The Journal of the Chemical Society*, 79, 3322.
- Kurbanov, M., Mamedov, K. F., 1995. The role of the reaction of CO + SH → COS + H. in hydrogen formation in the course of interaction between CO and H₂S. *Kinetics and catalysis*, 36, 455–457.
- Lee, J., Stief, L., Timmons, R., 1977. Absolute rate parameters for the reaction of atomic hydrogen with carbonyl sulfide and ethylene episulfide. *The Journal of Chemical Physics*, 67, 1705–1709.
- Lloyd, A. C., 1974. Evaluated and estimated kinetic data for phase reactions of the hydroperoxyl radical. *International Journal of Chemical Kinetics*, 6, 169–228.
- Martinez, R. I., Herron, J. T., 1983. Methyl thiirane: Kinetic gas-phase titration of sulfur atoms in S_xO_y systems. *International journal of chemical kinetics*, 15, 1127–1132.
- Moses, J., Fouchet, T., Bézard, B., Gladstone, G., Lellouch, E., Feuchtgruber, H., 2005. Photochemistry and diffusion in Jupiter's stratosphere: constraints from ISO observations and comparisons with other giant planets. *Journal of Geophysical Research: Planets*, 110.
- Perrin, D., Richard, C., Martin, R., 1988. Etude cinétique de la réaction thermique du pentène-2 cis vers 5000c. III: Influence de H₂S. *Journal de chimie physique*, 85, 185–192.

Sander, S. P., et al., 2006. Chemical kinetics and photochemical data for use in atmospheric studies evaluation number 15. JPL Publication 06–02.

Sander, S.P., et al., 2011. (JPL-11) Chemical Kinetics and Photochemical Data for Use in Atmospheric Studies – Evaluation Number 17. Jet Propulsion Laboratory Publication 10–6.

Schofield, K., 1973. Evaluated chemical kinetic rate constants for various gas phase reactions. Journal of Physical and Chemical Reference Data. 2, 25–84.

Shiina, H., Oya, M., Yamashita, K., Miyoshi, A., Matsui, H., 1996. Kinetic Studies on the Pyrolysis of H₂S. The Journal of Physical Chemistry. 100, 2136–2140.

Shum, L. G., Benson, S. W., 1985. The pyrolysis of dimethyl sulfide, kinetics and mechanism. International journal of chemical kinetics. 17, 749–761.

Singleton, D., Cvetanović, R. J., 1988. Evaluated chemical kinetic data for the reactions of atomic oxygen O (3P) with sulfur containing compounds. Journal of physical and chemical reference data. 17, 1377–1437.

Stachnik, R., Molina, M., 1987. Kinetics of the reactions of mercapto radicals with nitrogen dioxide and oxygen. Journal of Physical Chemistry. 91, 4603–4606.

Turco, R., Whitten, R., Toon, O., 1982. Stratospheric aerosols: Observation and theory. Reviews of Geophysics. 20, 233–279.

Yung, Y. L., DeMore, W., 1982. Photochemistry of the stratosphere of Venus: Implications for atmospheric evolution. Icarus. 51, 199–247.

Zahnle, K., Claire, M., Catling, D., 2006. The loss of mass-independent fractionation in sulfur due to a Palaeoproterozoic collapse of atmospheric methane. Geobiology. 4, 271–283.

Zahnle, K., Marley, M. S., Morley, C. V., Moses, J. I., 2016. Photochemical Hazes in the Atmosphere of 51 Eri b. Astrophysical Journal. *submitted*.

Appendix B. Surface sink on CO

Previous versions of this one-dimensional photochemical code have used a depositional velocity of 0 cm s⁻¹ on CO and 0.02 cm s⁻¹ on carbonyl sulfide (OCS) (Catling et al., 2010; Smith et al., 2014; Zahnle et al., 2008). However, in our high-outgassing rate atmospheres, volcanically sourced CO readily builds up in anoxic atmospheres. This is due in part to the assumptions of a cold, dry atmosphere similar to modern day Mars, where few OH radicals react with CO to produce redox neutral CO₂. Consequently, CO accumulates.

With the previous v_{dep} for CO and OCS, most of the carbon in the model (that is not removed as redox-neutral CO₂) deposits to the surface as OCS. This v_{dep} on OCS presents a couple of problems, as a) large amounts of OCS do not generally deposit on planetary surfaces and b) OCS begins to compete with S₈ for the available atmospheric sulfur in anoxic reducing conditions. While this did not matter in previous model versions, since OCS was a minor constituent, we reexamine the assumption here. On Earth, OCS sinks include vegetation (Brown and Bell, 1986) and soil microbes (Kesselmeier et al., 1999), which are irrelevant for an assumed abiotic Mars. A minor sink occurs from the reaction of OCS and OH at the surface; but this process is very slow on Earth (Khalil and Rasmussen, 1984), and would only be slower on Mars with even less OH available, especially in anoxic reducing conditions. Thus, it is more appropriate to use zero deposition velocity for OCS.

However, once the surface sink for OCS is removed, CO can build up at a rate that may not be reasonable given possible CO sinks. OCS is mostly formed through the net reactions:



When the sink for OCS is removed, atmospheric OCS photolyzes back into its products, CO and S, which leads to a greater amount of atmosphere CO.

There are possible surface sinks for CO. Gas-phase reactions involving CO are kinetically inhibited at low temperatures ($T < 1000$ K) due to the high activation energy barrier required to break the CO bond. Therefore, conversion of CO to other forms of carbon (e.g. CO₂ and CH₄) requires a catalyst and/or high temperatures in the absence of abundant OH. Hypervelocity impact events from large space debris (e.g. chondrites, iron-meteorites, and comets) create temporary conditions of high temperature and pressure in a vapor plume. In this plume, CO can adsorb onto iron and nickel particles from the impactor and participate in Fischer-Tropsch catalysis reactions that convert CO into CO₂ or CH₄:



Iron and nickel show a selectivity in their catalytic properties towards producing CH₄ over CO₂ (Eq. (B3)) (Kress and McKay, 2004). Such reactions are a sink on CO for early and modern Mars.

Kress and McKay (2004) describe the process of converting CO to CH₄ via the aforementioned process with comets. They show that comets of diameter (L) > 1 km produce $\sim 10^{13}$ g of CH₄ per impact, and furthermore impactors with $L > 10$ km produce $\sim 10^{15}$ g of CH₄. Thus, the total production of CH₄ from an impactor approximately depends on the square of the impactor radius. We use this dependency to approximate the distribution of fluxes from variously sized impactors and convert into photochemical model units of molecules of CH₄ produced per impact event. Also given that the conversion of CO to CH₄ is 1:1 (See Eq. (B3)), the same number of moles of CO will be removed via reaction B3 as moles of CH₄ are produced.

The number of impactors of diameter L impacting Mars can be estimated from the cratering record and scaling from crater diameter (D) to impactor diameter (L). From integrating the Hartmann and Neukum (2001) cratering rate over the past 4.1 Ga the average rate is $\sim 6.79 \times 10^{-11}$ impact events per second, or equivalently ~ 2.5 impacts every thousand years. This rate provides a first-order average approximation to the CO sink, although the sink is obviously higher in the Noachian than the late Amazonian, as discussed below.

The amount of CH₄ released is a function of impactor size. A relationship from Yen et al. (2006), derived from Melosh (1989), scales from crater diameter to impactor diameter, as follows:

$$D_{\text{crater}} = 1.8 \rho_{\text{proj}}^{0.11} \rho_{\text{target}}^{-1/3} g^{-0.22} L_{\text{impactor}}^{0.13} W^{0.22} \quad (\text{B.6})$$

Here, D_{crater} is the diameter of the crater, ρ_{proj} and ρ_{target} are the densities of the projectile and the target respectively, g is the gravitational acceleration of the target, L_{impactor} is the diameter of the impactor, and W is the impact kinetic energy (a function of the impact velocity, V). To first order $\rho_{\text{proj}} \sim \rho_{\text{target}}$ and the equation simplifies to the following:

$$L_{\text{impactor}} = 0.58 D_{\text{crater}}^{1.27} g^{0.28} V^{-0.56} \quad (\text{B.7})$$

Typical comet and asteroid impacts have mean speeds of around $V = 10$ km s⁻¹ (Bottke et al., 1994; Carr, 2006; Zahnle, 1998; Zahnle, 1990).

Robbins and Hynes (2012) provide a global database of craters on Mars greater than 1 km diameter as shown in Fig. B1 which is

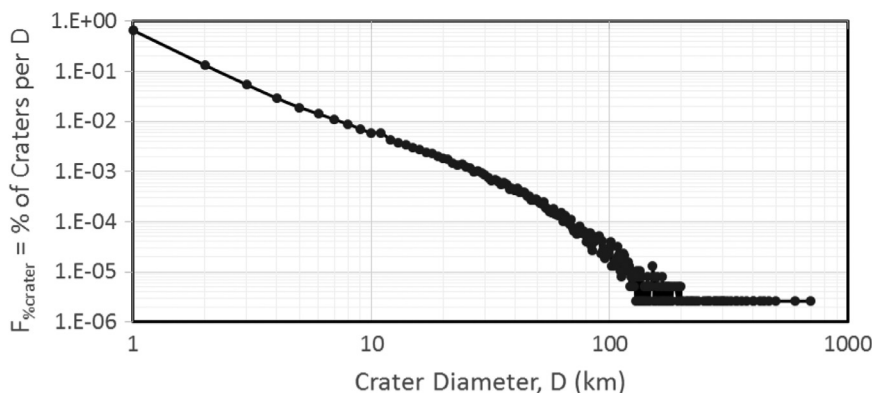


Fig. B.1. Distribution of craters, as a percentage of total craters, as a function of crater diameter for craters with diameters > 1 km. Each point represents a 1 km crater size bin which can be converted into impactor size using Eq. (B7). Craters with $D > \sim 200$ km have a frequency of only 1.

Table B1

Types of meteorites and the percentage of impacts on Earth. Efficiency correlates strongly with percentage of iron/nickel in the meteorite. Effective efficiency is the percentage of impacts (% of falls) multiplied by the efficiency of that body.

Meteorite type	% of falls	Efficiency	Effective efficiency, ϵ_i
Stony (chondrites)	93.8%	20% (max.)	18.8%
Stony/Iron	1.2%	50% (typical)	0.6%
Iron	5.0%	100%	5.0%
Total Effective Efficiency, ϵ			24.4%

used to determine impactor size distribution. This provides a first order estimate as degradation of larger craters could be a factor.

Finally, we must consider the efficiency of the impact chemistry. Kress and McKay (2004) present CH_4 production values for cometary bodies, which are a small fraction of the total impactor population. The majority of the impactors are stony ordinary chondrites. The smaller amount of iron and nickel present in ordinary chondrites makes them less efficient at catalytically converting CO to CH_4 . We take the percentage of iron and nickel in the meteorite to be a good estimate of the efficiency based on the work of Sekine et al. (2003); ordinary chondrites have 3–20% iron/nickel present and are 5–20% as efficient as purely iron and nickel meteorites in removing CO. Table B1 provides a list of meteorite types (stony, stony/iron, and iron) and their percentage of impacts on the Earth (Hutchison, 2004). We also provide an efficiency of each meteorite type based on the iron/nickel content and an effective efficiency for each type. Stony/iron meteorites, e.g. pallasites, contain iron contents ranging from 20 to 90% but we take 50% to represent a typical stony/iron meteorite. The total effective efficiencies of all three meteorite groups is 25%.

The total flux of CH_4 , F_{CH_4} (molecules $\text{cm}^{-2} \text{s}^{-1}$) into the atmosphere is then calculated using:

$$F_{\text{CH}_4} = \int_{0 \text{ km}}^{136 \text{ km}} \frac{f_{\text{flux}}(L) \times f_{\text{craters}}(L) \times \epsilon \times F_{\text{impacts}}}{A_{\text{Mars}}} dL \quad (\text{B.8})$$

Here, f_{flux} is the calculated CH_4 flux (in molecules/impact event) and is a function of impactor diameter as given in Kress and McKay (2004), f_{craters} is the percentage of craters per impactor size as given in Fig. B1, ϵ is the efficiency of the impactor as found in Table B1, F_{impacts} is the average flux of impactors over 4.1 Ga (6.79×10^{-11} impactors per second), and A_{Mars} is the surface area of Mars (in cm^{-2}). This is shown graphically in Fig. B2.

Integrating over the range of impactor sizes in Fig. B1 provides a total flux of CH_4 that is used as a lower boundary condition. The maximum crater size from the Robbins and Hynke (2012) database has a ~ 470 km diameter (Schiaparelli Crater), which corresponds

to an impactor size of ~ 85 km. However, their database does not include the larger buried craters in the northern plains. Thus we use the crater distribution from Frey et al. (2002) to include craters up to 700 km in diameter, corresponding to an impactor size of ~ 136 km. The authors find a quasi-circular depression (QCD), interpreted to be a large buried crater, of diameter 1075 km but we do not include this along with the other largest craters greater than Schiaparelli (Isidis, Argyre, and Hellas). These craters formed around the pre-Noachian/Noachian boundary (Werner, 2008) and represent very large impacts that appear to have only happened before ~ 3.9 – 4.1 Ga (Robbins et al., 2013). Given that surfaces are rarely older than this on Mars and that we wish to estimate the time-integrated average from Noachian surfaces and onwards, we ignore these anomalously large craters. To obtain the equivalent depositional velocity on CO, we use the number density of CO at the surface (for present day Mars) to calculate the downward flux of CO, $\Phi = v_{\text{dep}} n$. Here, v_{dep} is the deposition velocity, and n is the number density.

Meteoritic impact events can account for a time-average flux of CH_4 at the surface of $\sim 1 \times 10^7$ molecules $\text{cm}^{-2} \text{s}^{-1}$ and a corresponding deposition velocity on CO of $\sim 7.5 \times 10^{-8} \text{ cm s}^{-1}$. This is of the same order as the deposition velocity derived by Kharecha et al. (2005) for an abiotic ocean planet via the conversion of dissolved CO to formate and eventually acetate.

The change in cratering rate for each martian geologic period would cause the average CO sink to vary over time (Table B2). Today, the rate is virtually negligible at only $\sim 3 \times 10^{-9} \text{ cm s}^{-1}$, while during the early Noachian the rate was nearly 20 times faster than the average.

The availability of atmospheric H_2 or water-dissociated H_2 also plays a large factor in the efficiency of impact conversion of CO. We assume here that the impacts will happen either with sufficiently water-enriched bodies or impact on surface or subsurface reservoirs of water.

We performed multiple sensitivity tests to determine how much the deposition velocity on CO affects the overall chemistry

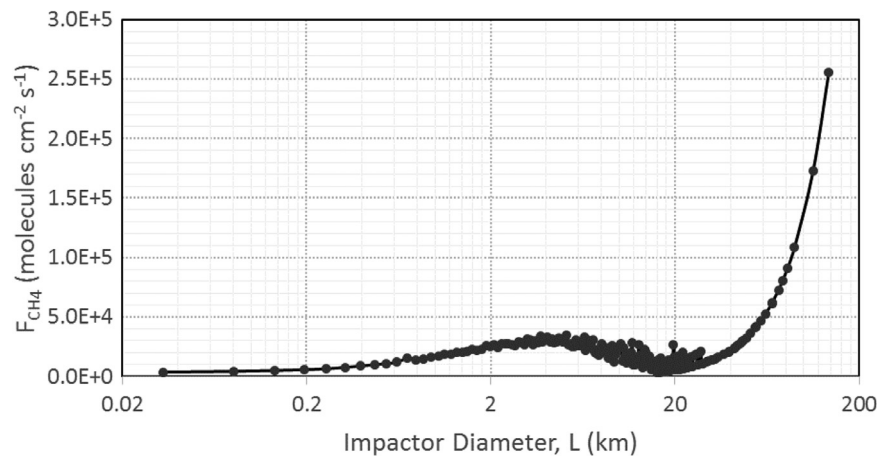


Fig. B.2. Flux of methane, F_{CH_4} , as a function of impactor diameter, L . For small impactors, $L < 18$ km, despite not producing much methane in each impact there are significantly more impacts occurring. Larger impacts are more infrequent but produce more methane.

Table B2

Comparison of CO deposition velocity, which depend on the cratering rate, over the geologic periods of Mars.

Era	Time	Cratering rate (impacts s^{-1})	$v_{\text{dep,CO}}$ (cm s^{-1})
Early Noachian	4.1 Ga	1.47×10^{-9}	1.39×10^{-6}
Early Hesperian	3.7 Ga	1.54×10^{-10}	1.46×10^{-7}
Early Amazonian	3.0 Ga	2.45×10^{-12}	2.32×10^{-9}
Mid Amazonian	1.0 Ga	2.33×10^{-12}	2.21×10^{-9}
Present	1 Ma	3.52×10^{-12}	3.33×10^{-9}
Average	–	6.79×10^{-11}	7.51×10^{-8}

and evolution of the modeled atmospheres. We find that deposition velocities of $0\text{--}10^{-7}\text{ cm s}^{-1}$ still produce modern martian conditions with no volcanic sources. They also show little change in the overall atmospheric evolution with increasing volcanic magma flux. Mixing ratios and depositional fluxes of all major constituents remain fairly uniform in magnitude. The only major difference is in the transitional atmospheres between oxidizing and reducing atmospheres where the steepness of the rise of CO with increasing volcanic flux becomes less sharp around $v_{\text{dep,CO}} = 10^{-7}\text{ cm s}^{-1}$. This, however does not change how much volcanism is required to produce the redox switch between the oxidizing and reducing atmospheres (see Eq. (5) in the main text). When the depositional velocity of CO becomes very large, on the order of 10^{-6} cm s^{-1} , the redox switch shifts towards requiring greater amounts of volcanism and the model is unable to adequately simulate present-day Mars. If the deposition velocity is too small, we encounter the CO-runaway numerical problem described at the beginning of this appendix.

Finally, other processes may have also contributed to a surface sink on CO. CO could very slowly adsorb onto surface iron and nickel (Kishi and Roberts, 1975; Rabo et al., 1978), dissolved CO could react directly with dissolved O_2 in surface waters (Harman et al., 2015), and CO may photodissociate into atomic C and O at a small rate and deposit on the surface or escape to space (Hu et al., 2015; Lu et al., 2014). Detailed consideration of all such processes is beyond the scope of this paper, but effectively, they could allow for the value of $v_{\text{dep,CO}}$ we have adopted.

Appendix B References

Bottke, W. F., Nolan, M. C., Greenberg, R., Kolvoord, R. A., 1994. Velocity distributions among colliding asteroids. *Icarus*. 107, 255–268.

Brown, K. A., Bell, J. N. B., 1986. Vegetation—The missing sink in the global cycle of carbonyl sulphide (COS). *Atmospheric Environment* (1967). 20, 537–540.

Carr, M. H., 2006. *The Surface of Mars*. Cambridge Univ. Press, Cambridge.

Catling, D. C., et al., 2010. Atmospheric origins of perchlorate on Mars and in the Atacama. *Journal of Geophysical Research: Planets*. 115, E00E11.

Frey, H. V., Roark, J. H., Shockey, K. M., Frey, E. L., Sakimoto, S. E., 2002. Ancient lowlands on Mars. *Geophysical Research Letters*. 29.

Harman, C. E., Schwieterman, E. W., Schottelkotte, J. C., Kasting, J. F., 2015. Abiotic O_2 Levels on Planets around F, G, K, and M Stars: Possible False Positives for Life? *The Astrophysical Journal*. 812, 137.

Hartmann, W. K., Neukum, G., 2001. Cratering chronology and the evolution of Mars. *Chronology and evolution of Mars*. Springer, pp. 165–194.

Hu, R., Kass, D. M., Ehlmann, B. L., Yung, Y. L., 2015. Tracing the fate of carbon and the atmospheric evolution of Mars. *Nature communications*. 6.

Hutchison, R., 2004. *Meteorites: A Petrologic, Chemical, and Isotopic Synthesis*. Cambridge University Press, Cambridge, UK.

Kesselmeier, J., Teusch, N., Kuhn, U., 1999. Controlling variables for the uptake of atmospheric carbonyl sulfide by soil. *Journal of Geophysical Research: Atmospheres*. 104, 11,577–11,584.

Khalil, M. A. K., Rasmussen, R. A., 1984. Global sources, lifetimes and mass balances of carbonyl sulfide (OCS) and carbon disulfide (CS_2) in the earth's atmosphere. *Atmospheric Environment* (1967). 18, 1805–1813.

Kharecha, P., Kasting, J. F., Siefert, J., 2005. A coupled atmosphere-ecosystem model of the early Archean Earth. *Geobiology*. 3, 53–76.

Kishi, K., Roberts, M. W., 1975. Carbon monoxide adsorption on iron in the temperature range 85 to 350 K as revealed by X-ray and vacuum ultraviolet [He (II)] photoelectron spectroscopy. *Journal of the Chemical Society, Faraday Transactions 1: Physical Chemistry in Condensed Phases*. 71, 1715–1720.

Kress, M. E., McKay, C. P., 2004. Formation of methane in comet impacts: implications for Earth, Mars, and Titan. *Icarus*. 168, 475–483.

Lu, Z., Chang, Y. C., Yin, Q.-Z., Ng, C., Jackson, W. M., 2014. Evidence for direct molecular oxygen production in CO_2 photodissociation. *Science*. 346, 61–64.

Melosh, H. J., 1989. *Impact cratering: A geologic process*. Research supported by NASA. New York, Oxford University Press (Oxford Monographs on Geology and Geophysics, No. 11), 1989, 253 p. 1.

Table C1

Nominal volcanic outgassing rates and speciation under varying magmatic conditions (water content, oxygen fugacity, and outgassing pressure) for a small amount of volcanism, $1 \times 10^{-4} \text{ km}^3 \text{ s}^{-1}$.

Magma conditions	Volcanic species flux [molecules $\text{cm}^{-2} \text{ s}^{-1}$]				
	SO ₂	S ₂	H ₂ S	CO	H ₂
IW					
0.01 wt% H ₂ O					
0.01 bar	1.2×10^5	1.0×10^6	4.7×10^4	2.5×10^6	6.0×10^5
1 bar	–	1.2×10^4	1.2×10^4	2.4×10^6	–
0.4 wt% H ₂ O					
0.01 bar	6.4×10^6	9.9×10^6	1.5×10^6	2.0×10^6	2.3×10^7
1 bar	1.5×10^6	2.1×10^6	3.9×10^6	1.3×10^6	1.2×10^7
FMQ-1.4					
0.01 wt% H ₂ O					
0.01 bar	2.5×10^6	6.7×10^6	4.7×10^4	5.2×10^6	4.0×10^5
1 bar	1.0×10^6	1.1×10^6	2.3×10^4	2.6×10^6	–
0.4 wt% H ₂ O					
0.01 bar	1.2×10^7	9.7×10^6	1.2×10^6	4.6×10^6	1.9×10^7
1 bar	4.9×10^6	3.7×10^6	3.5×10^6	2.6×10^6	8.4×10^6
FMQ-0.5					
0.1 wt% H ₂ O					
0.01 bar	8.2×10^6	9.5×10^6	4.2×10^5	4.9×10^6	4.6×10^6
1 bar	4.9×10^6	3.1×10^6	7.4×10^5	2.3×10^6	1.2×10^6
0.4 wt% H ₂ O					
0.01 bar	1.7×10^7	8.8×10^6	1.0×10^6	4.5×10^6	1.7×10^7
1 bar	8.5×10^6	4.4×10^6	3.1×10^6	2.4×10^6	7.2×10^6

Rabo, J., Risch, A., Poutsma, M., 1978. Reactions of carbon monoxide and hydrogen on Co, Ni, Ru, and Pd metals. *Journal of Catalysis*. 53, 295–311.

Robbins, S. J., Hynke, B. M., 2012. A new global database of Mars impact craters ≥ 1 km: 1. Database creation, properties, and parameters. *Journal of Geophysical Research: Planets* (1991–2012). 117.

Robbins, S. J., Hynke, B. M., Lillis, R. J., Bottke, W. F., 2013. Large impact crater histories of Mars: The effect of different model crater age techniques. *Icarus*. 225, 173–184.

Sekine, Y., Sugita, S., Kadono, T., Matsui, T., 2003. Methane production by large iron meteorite impacts on early Earth. *Journal of Geophysical Research: Planets* (1991–2012). 108.

Smith, M. L., Claire, M. W., Catling, D. C., Zahnle, K. J., 2014. The formation of sulfate, nitrate and perchlorate salts in the martian atmosphere. *Icarus*. 231, 51–64.

Werner, S., 2008. The early martian evolution—Constraints from basin formation ages. *Icarus*. 195, 45–60.

Yen, A. S., et al., 2006. Nickel on Mars: Constraints on meteoritic material at the surface. *Journal of Geophysical Research: Planets* (1991–2012). 111.

Zahnle, K., 1998. Origins of atmospheres. *Origins*, Vol. 148, pp. 364.

Zahnle, K., Haberle, R. M., Catling, D. C., Kasting, J. F., 2008. Photochemical instability of the ancient Martian atmosphere. *Journal of Geophysical Research: Planets*. 113, E11004.

Zahnle, K. J., 1990. Atmospheric chemistry by large impacts. *Geological Society of America Special Papers*. 247, 271–288.

Appendix C. Volcanic outgassing rates and ratios

For convenience, here we present a table showing the nominal volcanic outgassing rates calculated using Eq. (4) and sourced from Gaillard et al. (2013) (Table C1). These rates are given for a very small amount of volcanism, $1 \times 10^{-4} \text{ km}^3 \text{ s}^{-1}$, which represents the lowest values in Fig. 3. We only include fluxes for the maximum and minimum values of water content and outgassing pressure. As was described in Appendix B, we also include a static flux of 1×10^7 molecules $\text{cm}^{-2} \text{ s}^{-1}$ for CH₄ but this is negligible.

References

- Abelson, P.H., 1966. Chemical events on the primitive Earth. *Proc. Nat. Acad. Sci.* 55, 1365.
- Bar-Nun, A., Chang, S., 1983. Photochemical reactions of water and carbon monoxide in Earth's primitive atmosphere. *J. Geophys. Res.* 88, 6662–6672.
- Bar-Nun, A., Hartman, H., 1978. Synthesis of organic compounds from carbon monoxide and water by UV photolysis. *Origins Life* 9, 93–101.
- Batalha, N., Domagal-Goldman, S.D., Ramirez, R., Kasting, J.F., 2015. Testing the early Mars H₂-CO₂ greenhouse hypothesis with a 1-D photochemical model. *Icarus* 258, 337–349.
- Bibring, J.P., et al., 2005. Mars surface diversity as revealed by the OMEGA/Mars Express observations. *Science* 307, 1576–1581.
- Breuer, D., Spohn, T., 2006. Viscosity of the Martian mantle and its initial temperature: constraints from crust formation history and the evolution of the magnetic field. *Planet. Space Sci.* 54, 153–169.
- Brühl, C., Lelieveld, J., Crutzen, P., Tost, H., 2012. The role of carbonyl sulphide as a source of stratospheric sulphate aerosol and its impact on climate. *Atmos. Chem. Phys.* 12, 1239–1253.
- Burns, R.G., Fisher, D.S., 1993. Rates of oxidative weathering on the surface of Mars. *J. Geophys. Res.* 98, 3365–3372.
- Byrne, B., Goldblatt, C., 2014. Radiative forcings for 28 potential Archean greenhouse gases. *Clim. Past*. 10, 1779–1801.
- Carr, M.H., Head, J.W., 2010. Geologic history of Mars. *Earth Planet. Sci. Lett.* 294, 185–203.
- Catling, D.C., 1999. A chemical model for evaporites on early Mars: possible sedimentary tracers of the early climate and implications for exploration. *J. Geophys. Res.* 104, 16453–16469.
- Catling, D.C., 2009. Atmospheric Evolution, Mars. *Encyclopedia of Paleoclimatology and Ancient Environments*. Springer, pp. 66–75.
- Catling, D.C., 2014. Mars atmosphere: history and surface interactions. In: Spohn, T., Johnson, T.V., Breuer, D. (Eds.), *Encyclopedia of the Solar System*, second ed. Academic Press, New York in press.
- Catling, D.C., et al., 2010. Atmospheric origins of perchlorate on Mars and in the Atacama. *J. Geophys. Res.* 115, E00E11.
- Catling, D.C., Moore, J.M., 2003. The nature of coarse-grained crystalline hematite and its implications for the early environment of Mars. *Icarus* 165, 277–300.
- Chemtob, S.M., Nickerson, R.D., Morris, R.V., Agresti, D.G., Catalano, J.G., 2015. Synthesis and structural characterization of ferrous trioctahedral smectites: Implications for clay mineral genesis and detectability on Mars. *J. Geophys. Res.* 120 (6), 1119–1140.
- Chevrier, V., Poulet, F., Bibring, J.P., 2007. Early geochemical environment of Mars as determined from thermodynamics of phyllosilicates. *Nature* 448, 60–63.
- Claire, M.W., Kasting, J.F., Domagal-Goldman, S.D., Stüeken, E.E., Buick, R., Meadows, V.S., 2014. Modeling the signature of sulfur mass-independent fractionation produced in the Archean atmosphere. *Geochim. Cosmochim. Acta* 141, 365–380.
- Dehouck, E., Gaudin, A., Chevrier, V., Mangold, N., 2016. Mineralogical record of the redox conditions on early Mars. *Icarus* 271, 67–75.

- Domagal-Goldman, S.D., Meadows, V.S., Claire, M.W., Kasting, J.F., 2011. Using biogenic sulfur gases as remotely detectable biosignatures on anoxic planets. *Astrobiology* 11, 419–441.
- Ehlmann, B.L., et al., 2013. Geochemical consequences of widespread clay mineral formation in Mars' ancient crust. *Space Sci. Rev.* 174, 329–364.
- Ehlmann, B.L., et al., 2008. Orbital identification of carbonate-bearing rocks on Mars. *Science* 322, 1828–1832.
- Farquhar, J., Kim, S.T., Masterson, A., 2007. Implications from sulfur isotopes of the Nakhla meteorite for the origin of sulfate on Mars. *Earth Planet. Sci. Lett.* 264, 1–8.
- Fincham, C.J.B., Richardson, F.D., 1954. The behaviour of sulphur in silicate and aluminate melts. *Proc. R. Soc. London, Ser. A* 223, 40–62.
- Franz, H.B., et al., 2014. Isotopic links between atmospheric chemistry and the deep sulphur cycle on Mars. *Nature* 508, 364–368.
- Franz, H.B., et al., 2015. Reevaluated martian atmospheric mixing ratios from the mass spectrometer on the curiosity rover. *Planet. Space Sci.* 109, 154–158.
- Gaillard, F., Michalski, J., Berger, G., McLennan, S., Scailliet, B., 2013. Geochemical reservoirs and timing of sulfur cycling on Mars. *Space Sci. Rev.* 174, 251–300.
- Gaillard, F., Scailliet, B., 2009. The sulfur content of volcanic gases on Mars. *Earth Planet. Sci. Lett.* 279, 34–43.
- Gendrin, A., et al., 2005. Sulfates in martian layered terrains: the OMEGA/Mars Express view. *Science* 307, 1587–1591.
- Greeley, R., Schneid, B.D., 1991. Magma generation on Mars: amounts, rates, and comparisons with Earth, Moon, and Venus. *Science* 254, 996–998.
- Greeley, R., Spudis, P.D., 1981. Volcanism on Mars. *Rev. Geophys.* 19, 13–41.
- Halevy, I., Head, J.W., 2014. Episodic warming of early Mars by punctuated volcanism. *Nat. Geosci.* 7, 865–868.
- Halevy, I., Zuber, M.T., Schrag, D.P., 2007. A sulfur dioxide climate feedback on early Mars. *Science* 318, 1903–1907.
- Harder, H., 1978. Synthesis of iron layer silicate minerals under natural conditions. *Clays Clay Miner.* 26, 65–72.
- Harman, C.E., Schwietzman, E.W., Schottelkotte, J.C., Kasting, J.F., 2015. Abiotic O₂ levels on planets around F, G, K, and M stars: possible false positives for life? *Astrophys. J.* 812, 137.
- Hartmann, W.K., 2005. Martian cratering 8: isochron refinement and the chronology of Mars. *Icarus* 174, 294–320.
- Hausrath, E.M., Olsen, A.A., 2013. Using the chemical composition of carbonate rocks on Mars as a record of secondary interaction with liquid water. *Am. Mineral.* 98, 897–906.
- Herd, C.D.K., Borg, L.E., Jones, J.H., Papike, J.J., 2002. Oxygen fugacity and geochemical variations in the martian basalts: implications for martian basalt petrogenesis and the oxidation state of the upper mantle of Mars. *Geochim. Cosmochim. Acta* 66, 2025–2036.
- Hubbard, J.S., Hardy, J.P., Voeks, G.E., Golub, E.E., 1973. Photocatalytic synthesis of organic compounds from CO and water: involvement of surfaces in the formation and stabilization of products. *J. Mol. Evol.* 2, 149–166.
- Huber, C., Wächtershauser, G., 1998. Peptides by activation of amino acids with CO on (Ni,Fe) surfaces: implications for the origin of life. *Science* 281, 670–672.
- Johnson, A.P., Cleaves, H.J., Dworkin, J.P., Glavin, D.P., Lazzano, A., Bada, J.L., 2008a. The Miller volcanic spark discharge experiment. *Science* 322 404–404.
- Johnson, S.S., Mischna, M.A., Grove, T.L., Zuber, M.T., 2008b. Sulfur-induced greenhouse warming on early Mars. *J. Geophys. Res.* 113.
- Johnson, S.S., Pavlov, A.A., Mischna, M.A., 2009. Fate of SO₂ in the ancient martian atmosphere: implications for transient greenhouse warming. *J. Geophys. Res.* 114 E11011.
- Kasting, J.F., 1979. Evolution of Oxygen and Ozone in the Earth's Atmosphere. University of Michigan, p. 259.
- Kasting, J.F., 1993. Earth's early atmosphere. *Science* 259, 920–926.
- Kharecha, P., Kasting, J.F., Siefert, J., 2005. A coupled atmosphere-ecosystem model of the early Archean Earth. *Geobiology* 3, 53–76.
- King, P., McSween, H., 2005. Effects of H₂O, pH, and oxidation state on the stability of Fe minerals on Mars. *J. Geophys. Res.* 110.
- King, P.L., McLennan, S.M., 2010. Sulfur on Mars. *Elements* 6, 107–112.
- Kounaves, S.P., et al., 2010. Soluble sulfate in the martian soil at the Phoenix landing site. *Geophys. Res. Lett.* 37, L09201.
- Krasnopolsky, V.A., 2005. A sensitive search for SO₂ in the martian atmosphere: implications for seepage and origin of methane. *Icarus* 178, 487–492.
- Krasnopolsky, V.A., Lefevre, F., 2013. Chemistry of the atmospheres of Mars, Venus, and Titan. In: Mackwell, S.J., Simon-Miller, A.A., Harder, J.W., Bullock, M.A. (Eds.), *Comparative Climatology of Terrestrial Planets*. Univ. of Arizona Press, Tucson, pp. 231–275.
- Kress, M.E., McKay, C.P., 2004. Formation of methane in comet impacts: implications for Earth, Mars, and Titan. *Icarus* 168, 475–483.
- Leavitt, S., 1982. Annual volcanic carbon dioxide emission: an estimate from eruption chronologies. *Environ. Geol.* 4, 15–21.
- Leman, L., Orgel, L., Ghadiri, M.R., 2004. Carbonyl sulfide-mediated prebiotic formation of peptides. *Science* 306, 283–286.
- Li, J., Agee, C.B., 1996. Geochemistry of mantle-core differentiation at high pressure. *Nature* 381, 686–689.
- Mahaffy, P.R., et al., 2013. Abundance and isotopic composition of gases in the martian atmosphere from the curiosity rover. *Science* 341, 263–266.
- McAdam, A.C., et al., 2014. Sulfur-bearing phases detected by evolved gas analysis of the Rocknest aeolian deposit, Gale Crater, Mars. *J. Geophys. Res.* 119, 373–393.
- McGouldrick, K., Toon, O.B., Grinspoon, D.H., 2011. Sulfuric acid aerosols in the atmospheres of the terrestrial planets. *Planet. Space Sci.* 59, 934–941.
- McSween, H.Y., 1994. What we have learned about Mars from SNC meteorites. *Meteoritics* 29, 757–779.
- McSween, H.Y., et al., 2001. Geochemical evidence for magmatic water within Mars from pyroxenes in the Shergotty meteorite. *Nature* 409, 487–490.
- Michalski, J., Niles, P.B., 2010. Deep crustal carbonate rocks exposed by meteor impact on Mars. *Nat. Geosci.* 3 (11), 751–755.
- Michalski, J., Niles, P.B., 2012. Atmospheric origin of martian interior layered deposits: links to climate change and global sulfur cycle. *Geology* 40, 419–422.
- Miller, S.L., 1953. A production of amino acids under possible primitive Earth conditions. *Science* 117, 528–529.
- Miller, S.L., 1955. Production of some organic compounds under possible primitive Earth conditions. *J. Am. Chem. Soc.* 77, 2351–2361.
- Miller, S.L., 1986. Current status of the prebiotic synthesis of small molecules. *Chem Scr B* 26, 5–11.
- Miyakawa, S., Yamanashi, H., Kobayashi, K., Cleaves, H.J., Miller, S.L., 2002. Prebiotic synthesis from CO atmospheres: Implications for the origins of life. *Proc. Natl. Acad. Sci. U.S.A.* 99, 14628–14631.
- Morris, R.V., et al., 2010. Identification of carbonate-rich outcrops on Mars by the spirit rover. *Science* 329, 421–424.
- Murchie, S.L., et al., 2009. A synthesis of Martian aqueous mineralogy after 1 Mars year of observations from the Mars Reconnaissance Orbiter. *J. Geophys. Res.* 114, E00D06.
- O'Neill, H., Mavrogenes, J.A., 2002. The sulfide capacity and the sulfur content at sulfide saturation of silicate melts at 1400 °C and 1 bar. *J. Petrol.* 43, 1049–1087.
- Orgel, L.E., 1998. The origin of life—a review of facts and speculations. *Trends Biochem. Sci.* 23, 491–495.
- Parker, T.J., Gorsline, D.S., Saunders, R.S., Pieri, D.C., Schneeberger, D.M., 1993. Coastal geomorphology of the Martian northern plains. *J. Geophys. Res.* 98, 11061–11078.
- Pavlov, A.A., Kasting, J.F., 2002. Mass-independent fractionation of sulfur isotopes in Archean sediments: strong evidence for an anoxic Archean atmosphere. *Astrobiology* 2, 27.
- Peretyazhko, T., Sutter, B., Morris, R., Agresti, D., Le, L., Ming, D., 2016. Fe/Mg smectite formation under acidic conditions on early Mars. *Geochim. Cosmochim. Acta* 173, 37–49.
- Pinto, J.P., Gladstone, C.R., Yung, Y.L., 1980. Photochemical production of formaldehyde in the earth's primitive atmosphere. *Science* 210, 183–185.
- Postawko, S.E., Kuhn, W.R., 1986. Effect of the greenhouse gases (CO₂, H₂O, SO₂) on Martian paleoclimate. *J. Geophys. Res. (Proc. Lunar Planet. Sci. Conf. 16th)*, 91, D431–D438.
- Poulet, F., et al., 2005. Phyllosilicates on Mars and implications for early martian climate. *Nature* 438, 623–627.
- Ragsdale, S.W., 2004. Life with Carbon Monoxide. *Crit. Rev. Biochem. Mol. Biol.* 39, 165–195.
- Ramirez, R.M., Koppapu, R., Zuger, M.E., Robinson, T.D., Freedman, R., Kasting, J.F., 2014. Warming early Mars with CO₂ and H₂. *Nat. Geosci.* 7, 59–63.
- Robock, A., 2000. Volcanic eruptions and climate. *Rev. Geophys.* 38, 191–219.
- Ruff, S.W., Niles, P.B., Alfano, F., Clarke, A.B., 2014. Evidence for a Noachian-aged ephemeral lake in Gusev crater. *Mars. Geol.* 42, 359–362.
- Ryan, S., Dlugokencky, E.J., Tans, P.P., Trudeau, M.E., 2006. Mauna Loa volcano is not a methane source: Implications for Mars. *Geophys. Res. Lett.* 33 L12301.
- Sagan, C., 1977. Reducing greenhouses and the temperature history of Earth and Mars. *Nature* 269, 224–226.
- Schubert, G., Solomon, S.C., Turcotte, D.L., Drake, M.J., Sleep, N.H., 1992. Origin and thermal evolution of Mars. In: H. H. Kieffer, B. M. Jakosky, C. W. Snyder, M. S. Matthews, (Eds.), *Mars*. The University of Arizona Press, Tucson, AZ.
- Sekine, Y., Sugita, S., Kadono, T., Matsui, T., 2003. Methane production by large iron meteorite impacts on early Earth. *J. Geophys. Res.* 108, 1991–2012.
- Settle, M., 1979. Formation and deposition of volcanic sulfate aerosols on Mars. *J. Geophys. Res.* 84, 8343–8354.
- Smith, M.L., Claire, M.W., Catling, D.C., Zahnle, K.J., 2014. The formation of sulfate, nitrate and perchlorate salts in the martian atmosphere. *Icarus* 231, 51–64.
- Squyres, S.W., et al., 2004. In situ evidence for an ancient aqueous environment at meridiani planum, Mars. *Science* 306, 1709–1714.
- Symonds, R.B., Rose, W.I., Bluth, G.J.S., Gerlach, T.M., 1994. Volcanic-gas studies: methods, results, and applications. *Rev. Mineral. Geochem.* 30, 1–66.
- Tian, F., et al., 2010. Photochemical and climate consequences of sulfur outgassing on early Mars. *Earth Planet. Sci. Lett.* 295, 412–418.
- Tian, F., Toon, O.B., Pavlov, A.A., De Sterck, H., 2005. A hydrogen-rich early Earth atmosphere. *Science* 308, 1014–1017.
- Toon, O.B., Turco, R.P., Pollack, J.B., 1982. The ultraviolet absorber on Venus: amorphous sulfur. *Icarus* 51, 358–373.
- Toulmin, P., et al., 1977. Geochemical and mineralogical interpretation of the Viking inorganic chemical results. *J. Geophys. Res.* 82, 4625–4634.
- Ueno, Y., Johnson, M.S., Danielache, S.O., Eskebjerg, C., Pandey, A., Yoshida, N., 2009. Geological sulfur isotopes indicate elevated OCS in the Archean atmosphere, solving faint young sun paradox. *Proc. Natl. Acad. Sci.* 106, 14784–14789.
- Urey, H.C., 1952. On the Early Chemical History of the Earth and the Origin of Life. *Proc. Natl. Acad. Sci. U.S.A.* 38, 351–363.
- Velde, B., 1992. Introduction to Clay Minerals: Chemistry, Origins, Uses and Environmental Significance. Chapman & Hall, London, UK.
- Wänke, H., Dreibus, G., 1994. Chemistry and accretion history of Mars. *Phil. Trans. R. Soc. Lond. A* 349, 285–293.
- Werner, S., Tanaka, K., 2011. Redefinition of the crater-density and absolute-age boundaries for the chronostratigraphic system of Mars. *Icarus* 215, 603–607.

- Werner, S.C., 2009. The global martian volcanic evolutionary history. *Icarus* 201, 44–68.
- Wetzel, D.T., Rutherford, M.J., Jacobsen, S.D., Hauri, E.H., Saal, A.E., 2013. Degassing of reduced carbon from planetary basalts. *Proc. Natl. Acad. Sci.* 110, 8010–8013.
- Wignall, P.B., 2001. Large igneous provinces and mass extinctions. *Earth-Sci. Rev.* 53, 1–33.
- Wordsworth, R.D., Kerber, L., Pierrehumbert, R.T., Forget, F., Head, J.W., 2015. Comparison of “warm and wet” and “cold and icy” scenarios for early Mars in a 3-D climate model. *J. Geophys. Res.* 120, 1201–1219.
- Xiao, L., et al., 2012. Ancient volcanism and its implication for thermal evolution of Mars. *Earth Planet. Sci. Lett.* 323–324, 9–18.
- Yen, A.S., et al., 2005. An integrated view of the chemistry and mineralogy of Martian soils. *Nature* 436, 49–54.
- Zahnle, K., Claire, M., Catling, D., 2006. The loss of mass-independent fractionation in sulfur due to a Palaeoproterozoic collapse of atmospheric methane. *Geobiology* 4, 271–283.
- Zahnle, K., Haberle, R.M., Catling, D.C., Kasting, J.F., 2008. Photochemical instability of the ancient Martian atmosphere. *J. Geophys. Res.* 113, E11004.
- Zahnle, K., Marley, M.S., Morley, C.V., Moses, J.I., 2016. Photolytic Hazes in the Atmosphere of 51 Eri b. *The Astrophysical Journal*. 824, 137.
- Zahnle, K.J., 1986. Photochemistry of methane and the formation of hydrocyanic acid (HCN) in the Earth's early atmosphere. *J. Geophys. Res.* 91, 2819–2834.